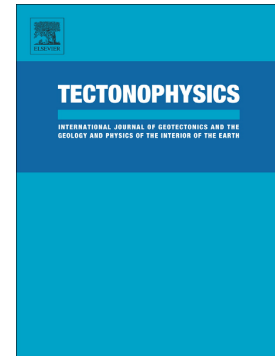


Accepted Manuscript

Late Quaternary strike-slip along the Taohuala Shan-Ayouqi fault zone and its tectonic implications in the Hexi Corridor and the southern Gobi Alashan, China

Yu Jing-xing, Zheng Wen-jun, Zhang Pei-zhen, Lei Qi-yun, Wang Xu-long, Wang Wei-tao, Li Xin-nan, Zhang Ning



PII: S0040-1951(17)30390-6
DOI: doi:[10.1016/j.tecto.2017.09.014](https://doi.org/10.1016/j.tecto.2017.09.014)
Reference: TECTO 127627
To appear in: *Tectonophysics*
Received date: 9 May 2017
Revised date: 21 August 2017
Accepted date: 19 September 2017

Please cite this article as: Yu Jing-xing, Zheng Wen-jun, Zhang Pei-zhen, Lei Qi-yun, Wang Xu-long, Wang Wei-tao, Li Xin-nan, Zhang Ning , Late Quaternary strike-slip along the Taohuala Shan-Ayouqi fault zone and its tectonic implications in the Hexi Corridor and the southern Gobi Alashan, China. The address for the corresponding author was captured as affiliation for all authors. Please check if appropriate. Tecto(2017), doi:[10.1016/j.tecto.2017.09.014](https://doi.org/10.1016/j.tecto.2017.09.014)

This is a PDF file of an unedited manuscript that has been accepted for publication. As a service to our customers we are providing this early version of the manuscript. The manuscript will undergo copyediting, typesetting, and review of the resulting proof before it is published in its final form. Please note that during the production process errors may be discovered which could affect the content, and all legal disclaimers that apply to the journal pertain.

Late Quaternary strike-slip along the Taohuala Shan-Ayouqi fault zone and its tectonic implications in the Hexi Corridor and the southern Gobi Alashan, China

Yu Jing-xing^{a,b}, Zheng Wen-jun^c, Zhang Pei-zhen^{a,c}, Lei Qi-yun^d, Wang Xu-long^e, Wang Weitao^a, Li Xin-nan^a, Zhang Ning^f

^a State Key Laboratory of Earthquake Dynamics, Institute of Geology, China Earthquake Administration, Beijing 100029, China

^b COMET, Department of Earth Sciences, University of Oxford, Oxford OX1 3AN, UK

^c School of Earth Science and Geological Engineering, Sun Yat-Sen University, Guangzhou 510275, China

^d Earthquake Administration of Ningxia Hui Autonomous Region, Yinchuan 750001, China

^e State Key Laboratory of Loess and Quaternary Geology, Institute of Earth Environment, Chinese Academy of Sciences, Xi'an 710075, China

^f Earthquake Administration of Hainan Province, Haikou 570100, China

ABSTRACT

The Hexi Corridor and the southern Gobi Alashan are composed of discontinuous a set of active faults with various strikes and slip motions that are located to the north of the northern Tibetan Plateau. Despite growing understanding of the geometry and kinematics of these active faults,

the late Quaternary deformation pattern in the Hexi Corridor and the southern Gobi Alashan remains controversial. The active E-W trending Taohuala Shan-Ayouqi fault zone is located in the southern Gobi Alashan. Study of the geometry and nature of slip along this fault zone holds crucial value for better understanding the regional deformation pattern. Field investigations combined with high-resolution imagery show that the Taohuala Shan fault and the E-W trending faults within the Ayouqi fault zone (F2 and F5) are left-lateral strike-slip faults, whereas the NW or WNW-trending faults within the Ayouqi fault zone (F1 and F3) are reverse faults. We collected Optically Stimulated Luminescence (OSL) and cosmogenic exposure age dating samples from offset alluvial fan surfaces, and estimated a vertical slip rate of 0.1-0.3 mm/yr, and a strike-slip rate of 0.14-0.93 mm/yr for the Taohuala Shan fault. Strata revealed in a trench excavated across the major fault (F5) in the Ayouqi fault zone and OSL dating results indicate that the most recent earthquake occurred between ca. 11.05 ± 0.52 ka and ca. 4.06 ± 0.29 ka. The geometry and kinematics of the Taohuala Shan-Ayouqi fault zone enable us to build a deformation pattern for the entire Hexi Corridor and the southern Gobi Alashan, which suggest that this region experiences northeastward oblique extrusion of the northern Tibetan Plateau. These left-lateral strike-slip faults in the region are driven by oblique compression but not associated with the northeastward extension of the Altyn Tagh fault.

Keywords: Fault Geometry; Active Tectonics; Hexi Corridor; Gobi Alashan; Northeastern Tibetan Plateau

1. Introduction

The Hexi Corridor, 700 km long and 50-100 km wide, is an active foreland basin located in the transitional zone between the northern Tibetan Plateau and the Gobi Alashan Block (Fig. 1a). To the south of the Hexi Corridor, the Qilian Shan (Shan = mountain) is characterized by intense crustal shortening, forming active mountain ranges and intramontane basins with high elevations of up to 5500 m (Meyer et al., 1998; Tapponnier et al., 1990, 2001; Yin et al., 2000, 2002). To the north, the inner Gobi Alashan block is tectonically inactive in the late Cenozoic, and is covered by aeolian deposits of the Badain Jaran and Tengger Deserts with a mean elevation of 1300 m (Tapponnier and Molnar, 1977; Xu et al., 2010; Yu et al., 2016) (Fig. 1a). Located in the transitional zone between these two distinct tectonic regimes, the Hexi Corridor and southern Gobi Alashan have a set of active faults with several historical earthquakes (Xu et al., 2010). Determination of the geometry and kinematics of these active faults is important for understanding the late Quaternary deformation pattern of the Hexi Corridor, southern Gobi Alashan, and northernmost Tibetan Plateau. Two influential views of the deformation pattern in the Hexi Corridor and southern Gobi Alashan have been debated for decades: 1) The faults in the Hexi Corridor and southern Gobi Alashan constitute a strike-slip fault system that transfers left-lateral strike slip along the Altyn Tagh fault into the inner Gobi Alashan Block and further east to eastern Mongolia (Yue and Liou, 1999; Darby et al., 2005; Webb and Johnson, 2006). This view predicts that most of the faults in the Hexi Corridor and southern Gobi Alashan are left-lateral strike-slip faults. Although the result is supported by sparse geological data of Mesozoic and early Cenozoic offsets from southern Mongolia and the Gobi Alashan Block (Webb and Johnson, 2006; Darby et al., 2005), it remains ambiguous whether or not these offsets are associated with the Altyn Tagh fault. 2) The northern Tibetan Plateau extrudes northeastward and the active faulting in the Hexi Corridor and southern Gobi Alashan represents the

northeastern boundary of the plateau (Tapponnier et al., 1990; Meyer et al., 1998; Zheng et al., 2013a). It predicts that most of the faults in this region are reverse faults. These reverse faults act as splay faults of a decollement at depth that extends into underneath northern Tibet.

Current published studies suggest that the faults in the Hexi Corridor and southern Gobi Alashan are thrust faults (e.g., Min et al., 2002; Hetzel et al., 2002, 2004; Zheng et al., 2013a, b).

However, a studies based on the satellite imagery and field investigations, showing that the active faults in this regions have an apparent strike-slip component, e.g., Jinta Nan Shan fault (Zheng, 2009; Zhang et al., 2016a), but nearly no detailed field investigation on most of these strike-slip faults has been conducted yet. In this paper, we present a geological and geomorphic study of the late Quaternary activity of the Taohuala Shan-Ayouqi fault zone in the southern Gobi Alashan. Based on high-resolution satellite imagery and field geomorphic mapping, we unravel the geometry of the fault zone. Meanwhile, for the determination of fault motion we studied displaced geomorphological features, such as offset streams, shutter ridges, pressure ridges, hill-facing fault scarps, and fault geometry in shallow surfaces. We also use geochronology (OSL and cosmogenic exposure age dating) to determine the slip rates and rupture timing of recent fault rupture events. The deformation pattern of the Taohuala Shan-Ayouqi fault zone is crucial for the better understanding of the late Quaternary deformation of the entire Hexi Corridor and the southern Gobi Alashan.

2. Geological setting

The Gobi Alashan Block is a tectonically inactive platform bounded by the Tibetan Plateau, Ordos Block, Tarim Block, and Gobi Altai in the south, east, west, and north direction respectively. Most of the region is covered by the third and fourth largest deserts of China, the Badain Jaran and Tengger Deserts. Exposed rocks in this region are mainly Precambrian metamorphic rocks, Paleozoic granite, and Mesozoic conglomerates (BGMRG, 1989). Extensional basins and metamorphic core complexes indicate that the Gobi Alashan Block experienced regional extension during the late Mesozoic (Kimura et al., 1990; Vincent and Allen, 1999; Zorin et al., 1995; Meng, 2003). As the Cenozoic deposits only accumulated in several basins and range fronts, it was thought that the block has been slowly uplifted during the Cenozoic (BGMRG, 1989). No earthquake with magnitude larger than 6 is recorded in the Gobi Alashan to provide insight into regional tectonics (Xu et al., 2010). Recently, based on geomorphological expressions and trench exposures along the Yabrai fault, Yu et al., (2016) suggest that the northeastward oblique extrusion of the Tibetan Plateau played a crucial role in the late Quaternary deformation in the Gobi Alashan Block.

The Hexi Corridor Basin, which is an asymmetrical foreland basin that mainly is controlled by subsidence in the footwall of the Northern Qilian thrust fault, is separated from the Gobi Alashan Block to the north by a row of relatively low topographic mountain ranges, including the Jinta Nan Shan, Heli Shan, Beida Shan, and Longshou Shan and these mountain ranges are bounded by active faults. The Longshou Shan, which is the northern boundary of the eastern Hexi Corridor, is associated with the largest earthquake recorded in the southern Gobi Alashan, the 1954 $M_{7.1/4}$ Shandan Earthquake (Zheng et al., 2013c). Field observations suggest that the earthquake ruptured the north Longshou Shan fault for a length of 7 km. Along the northern and

southern flanks of the mountain range, less evidence for late Quaternary activity have been recorded. The most continuous active fault, the Taohuala Shan fault, lies along the frontal range of the Taohuala Shan which is a small mountain in the northwestern corner of the Longshou Shan (Fig. 1b). Further north into the Gobi Alashan Block, the Mesozoic-Cenozoic Chaoshui Basin (Vincent and Allen, 1999), separates the Longshou Shan and the eastern end of the Beida Shan. Several other important active faults constitute the Ayouqi fault zone, cutting the Paleozoic granite at the eastern end of the Beida Shan. Here, we document the geometry and slip along the Taohuala Shan fault and the Ayouqi fault zone, determine late Quaternary slip rates, and discuss the deformation pattern of the Taohuala Shan-Ayouqi fault zone and its tectonic implications.

3. Methods

3.1 Detailed mapping using high-resolution satellite imagery and Structure from Motion (SfM) technique

High-resolution satellite imagery (WorldView and Pleiades Satellite imagery with a spatial resolution of ~0.5 m) were used to interpret the characteristics of fault scarps and slip motions (e.g., Zhou et al., 2015). Differences in geomorphic expression between primarily dip-slip and strike-slip faults may not be solely due to the heterogeneous materials of the crust, but also the complexity of surface ruptures during an earthquake (Burbank and Anderson, 2012). In strike-slip faulting, step-overs are commonly present, in which one segment of the fault trace ends and a second commences with the same sense of motion. The complicated array of structures within

step-over zone is determined by a combination of the sense of motion on the major relatively straight strike-slip fault and the geometry of the step-over zone. Other well-known geomorphological features, such as linear troughs, offset streams, uphill fault scarps, shutter ridges, pressure ridges, and beheaded streams, etc., commonly form along strike-slip fault traces (Burbank and Anderson, 2012). In contrast, active dip-slip faults typically form more sinuous and disrupted fault scarps in unconsolidated late Quaternary deposits with remarkable vertical displacement and absence of significant strike slip. In map view, dip-slip faults usually extend along asymmetric ranges with one steep, fault-bounded flank and a gently sloping opposite flank.

At some key sites, high-resolution (up to 0.1 m) imagery and Digital Elevation Models (DEMs) were prepared using a small Unmanned Aerial Vehicle (UAV) Motaar Sky MS670 with a SONY QX-1 camera. Photographs were collected from an altitude of ~30 m with sufficient overlaps (70%). We also collected ground control points using differential GPS with a density of 10 points per square kilometer. SfM point clouds, DEMs, and orthoimages were built using Agisoft Photoscan (Johnson et al., 2014). Displacements were measured based on the DEMs. We used a global navigation satellite system (GNSS, Trimble R8) differential positioning system to determine vertical displacements across active fault scarps on alluvial-fan surfaces. Vertical separations on well-preserved alluvial surfaces were derived from the topographic profiles perpendicular to the fault scarps (Hanks, 2000; Thompson et al., 2002)

3.2 Fault geometry exposed in trenches

To investigate fault geometry at shallow depth and large earthquake occurrence, three trenches were excavated by hand digging or a tracked excavator. After digging, we equipped the faces with a 1-m-spaced cord grid and then logged the strata and fault zone at 1:20 scale for the exposed walls. Fault geometry in trenches enables us to explore whether the fault experienced an extension or shortening. Besides basic criteria of fault-slip motions based on relative slip in different blocks of fault planes, normal faults are more likely to have secondary faults and fissures filled with rubble, whereas gouge, slickensides, breccia, crushing, or polishing present more likely in reverse faults (Bonilla and Lienkaemper, 1991; McCalpin, 2009). Both normal and reverse faulting may appear in different trenches along a strike-slip fault. Then, combining the geometry revealed in trenches and geomorphological features, we could determine slip motions on active faults.

3.3 Geochronology

In situ-produced cosmogenic nuclide (^{10}Be) exposure age and Optically Stimulated Luminescence (OSL) dating were employed to constrain exposure ages of alluvial fans and depositional ages of layers in trenches, respectively. In the field, we selected well-preserved alluvial surfaces where the influence of erosion and reworking is negligible. Clasts in diameter of ~2-3 cm on these alluvial surfaces were collected for ^{10}Be dating. ^{10}Be samples were processed and tested at the Xi'an Accelerator Mass Spectrometry Centre (XAAMS). The quartz was separated and purified using the method of Kohl and Nishiizumi (1992) and the production rates of ^{10}Be were scaled to the locations of sampling sites using the procedure of Lal (1991). Sample

ages were calculated using the online CRONUS calculator (Balco et al., 2008). Cosmogenic nuclide (^{10}Be) exposure age dating results are present in Table 1.

OSL samples were collected in opaque stainless tubes and further analysis was carried out at the State Key Laboratory of Loess and Quaternary Geology, Institute of Earth Environment, Chinese Academy of Sciences in Xi'an. Removing both ends of the samples in stainless tubes under subdued red lighting in OSL dating laboratory, the inner part of fresh portions were used for equivalent dose (ED) determination, and the remaining were used for the estimation of water content, and the analyses of U, Th, and K_2O . Fine-grained ($4\text{-}11\mu\text{m}$) or coarse ($90\text{-}125\mu\text{m}$) quartz grains were prepared for ED measurements by the sensitivity-corrected multiple aliquot regenerative dose (SMAR) protocol (Lu *et al.*, 2007) or single aliquot regenerative dose (SAR) protocol (Murray and Wintle, 2000). All OSL measurements were carried on a Daybreak 1100 or 2200 OSL system equipped with a combined blue ($470 \pm 5\text{ nm}$) and infrared ($880 \pm 8\text{ nm}$) LED unit, and a $^{90}\text{Sr}/^{90}\text{Y}$ beta source for irradiation. The U and Th concentration were measured on ICP-MS and the K was on ICP-OES. All OSL dating results and related information are present in Table 2.

4. Taohuala Shan fault

The Taohuala Shan fault, located in the northwestern corner of the Longshou Shan, extends E-W for ~30 km along the range front. South of the fault is the mountain range mainly composed of Precambrian gneiss, and Cretaceous and Neogene terrestrial deposits (GBGMR, 1971). The north side of the fault is composed of alluvial deposits. Based on the geometry of the fault at the

surface and variation in strike direction, we divided it into three segments, i.e. the western segment, step-over zone, and eastern segment (Fig. 2a). The western and eastern segments are characterized by left-lateral strike-slip motion. The eastern end shows predominant reverse motion. Several sub-parallel fault scarps are distributed between these two segments, indicative of a step-over zone along a strike-slip fault. Combining displacements across the fault scarps and dating of alluvial surfaces (OSL and cosmogenic exposure age dating), we estimate a left-lateral strike-slip rate of 0.14-0.93 mm/yr, and a vertical slip rate of 0.1-0.3 mm/yr.

4.1 Western segment

The western segment extends for ~20 km, showing continuous linear fault scarps along the range front in satellite imagery (Fig. 2a). At the western end of the western segment, the fault displaces Precambrian gneiss for at least 7 km in a left-lateral sense. The Cretaceous sandstones, however, are not displaced (GBGMR, 1971) (Fig. 1b), suggesting that significant left-lateral strike slip occurred along this fault in the pre-Cretaceous. Along the fault trace, a body of evidence indicates that the western segment of the fault is characterized by left-lateral strike slip in the late Quaternary as described below (Figs. 2b-e).

At Site 1 ($39^{\circ}11'36.52''N$, $100^{\circ}57'40.57''E$), two alluvial fans have been displaced by a single fault trace (Fig. 2b). In the west of the site, two small streams developed on the lower alluvial-fan surface are displaced by ~2-4 m in a left-lateral sense of motion, whereas the field investigations show that the vertical displacement across the fault scarp is less than 0.5 m. In the east of the site, an uphill-facing fault scarp developed on the higher alluvial fan forms a shutter

ridge to deflect the northward-flowing streams into eastward flowing. The fault trace extends continuously along the range front to Site 2 ($39^{\circ}11'35.11''N$, $100^{\circ}59'34.05''E$) (Fig. 2c). A pressure ridge, ~50 m long and 5 m wide, is developed parallel to the fault trace. A stream across the pressure ridge is displaced by ~4-5 m in a left-lateral sense of motion. In the east of Site 2, the heavily eroded higher alluvial-fan surface is truncated by the fault with a south facing fault scarp, and a north-south gully is displaced by 47 ± 3 m. Site 3 ($39^{\circ}11'39.82''N$, $101^{\circ}0'6.75''E$), ~700 m farther east of Site 2, also shows evidence for left-lateral strike slip (Fig. 2d). Two sub-parallel fault scarps displace alluvial-fan surfaces. Three streams are offset in a left-lateral sense of slip by the northern strand with displacements of 8 ± 2 m, 8.5 ± 2 m, and 16 ± 3 m, respectively. The vertical displacement is less than a meter across both the strands. Site 4 ($39^{\circ}11'46.51''N$, $101^{\circ}2'30.82''E$) is located ~3.4 km east of Site 3 (Fig. 2e). Remnants of an alluvial-fan surface are displaced by the fault. Two gullies incised into the surface are offset by 19.1 ± 1.5 m and 43 ± 6 m, significantly larger than the vertical displacements (1-3 m).

Our observations of the geomorphic features along the fault trace, including the left-laterally offset streams, pressure ridges, shutter ridges, and hill-facing scarps, suggest that the western segment of the Taohuala Shan fault is characterized by left-lateral strike-slip motion.

Unfortunately, due to the heavy erosion of the alluvial fan surfaces near the range front in this segment, it is not possible to carry out dating and so we are unable to provide an estimate of fault slip rate.

4.2 Step-over zone

Farther east, the fault in the step-over zone bends to be WNW-ESE striking and the fault trace is divided into several sub-parallel strands (Figs. 2a and 3). Based on our field geological investigations and interpretations of satellite imagery, six remnant alluvial terraces (T0-T5) are mapped along this segment (Figs. 3a, b). Except for the present channels and active alluvial fan (T0), all the other higher alluvial levels are displaced by the fault. The alluvial fan T1 is the most extensive and has been displaced by three strands of fault scarps facing different directions. The two remnant alluvial fans (T2, T3), whose footwalls are covered by T1, are only preserved near the range front. The two highest alluvial fans (T4, T5) are well preserved with several strands of fault scarps. There are 8 strands of fault scarp present on the T4 surface and 10 on the T5 surface. Among these fault scarps, the northernmost three strands on T5 (two on T4) face to the north and all the others are south-facing. To determine how these fault scarps developed, we undertook detailed geological mapping of the attitudes of fault planes and sedimentary bedding near the shallow surfaces of T4 and T5. The bedding dips to the NE and strikes WNW-ESE (Fig. 3b), which is consistent with the attitudes of the fault planes under the south-facing fault scarps that are revealed by fault gouge (Figs. 3c, d). The geometry of the fault splays near the shallow surfaces of T4 and T5 may indicate a flower structure at depth at this site (Fig. 3e). Although a simple flower structure cannot explain the distribution and facing directions of all the fault scarps, the complex geometry and change in strike of these fault scarps suggest that this site experiences transpressional deformation between the western and eastern segments of the strike-slip Taohuala Shan fault.

4.3 Eastern segment

To the east of the step-over zone, all strands of the fault merge into one single major fault trace that extends for ~8 km with a strike of WNW-ESE (Fig. 2a). Between the step-over zone and Site 6, the fault cuts alluvial-fan surfaces with no significant vertical displacement. However, to the east of Site 6, the fault is characterized by dip-slip faulting with remarkable fault scarps on alluvial fans. In the west of Site 6, the fault trace lies between Cretaceous and Neogene sandstones with vertical offset less than 0.5 m (Figs. 4a-c). In the east, two strands of the fault scarps vertically displace a widely distributed alluvial-fan surface by ~3-5 m (Figs. 4a, b). A pressure ridge along the southern strand is present, and a stream across the ridge and the riser of the alluvial fan are left-laterally displaced by ~26 m (Fig. 4d). Three small streams soon to the east of these features are also offset by ~4 m (Figs. 4e, f). To estimate the late Quaternary slip rate of the fault, we collected an OSL sample (Yu-15-OSL-001) from a lens of fine sands at a depth of 0.95 m (Fig. 4g). The sample yielded an age of 27.9 ± 1.09 ka (Table 2). Dividing the vertical displacements across the fault scarps by the OSL age, we estimate a vertical slip rate of the southern and northern strands of the fault of 0.12 ± 0.02 mm/yr, 0.17 ± 0.04 mm/yr, respectively. Thus, the total vertical slip rate is ~0.3 mm/yr. Dividing the lateral displacements of the streams and the riser of the alluvial fan by the dating result, we derived a left-lateral strike-slip rate of between 0.14 ± 0.01 mm/yr and 0.93 ± 0.11 mm/yr.

At Site 7, five alluvial fans (T1-T5) are preserved on the eastern bank of a river (Figs. 5a, b). T1 is the youngest and most extensive alluvial fan that is preserved on both flanks of the fault, and all the other four fans (T2-T5) are only preserved on the southern side of the fault (Figs. 5b, c). A single fault trace displaces all five alluvial fan levels but the present channel and floodplain (T0)

are not displaced. A natural exposure on the western wall of the river reveals several fault branches that juxtapose Neogene sandstones over late Quaternary alluvial gravels (Fig. 5d), indicative of a reverse component. Topographic profiles across the fault scarps, which are derived from differential GPS measurements, show that vertical displacements of the five alluvial fan levels (T1-T5) are 1.7 ± 0.4 m, 3.9 ± 0.2 m, 4.3 ± 2.0 m, 4.8 ± 0.7 m, and 20 ± 0.5 m, respectively (Fig. 5e). As the downthrown walls of the four higher fans (T2-T5) are covered by T1, these displacements only give a minimum value of dip slip. We failed to extract enough quartz grains for the sample from the active channel to estimate the inherited component nuclide concentration, so we derived the maximum exposure ages of the five fans (T1-T5) to be 29.8 ± 2.7 ka, 59.2 ± 5.1 ka, 57.1 ± 4.9 ka, 67.4 ± 5.9 ka, and 137.1 ± 12.0 ka, respectively (Table 1). Thus, with the minimum displacements and maximum exposure ages of the five alluvial fans, we estimate the minimum vertical slip rate to be 0.07-0.15 mm/yr at this site.

5. Ayouqi fault zone

The Ayouqi fault zone is composed of seven discontinuous active faults (F1-F7) with different senses of motion and trends (Fig. 6). Amongst them, faults F1 and F3, striking NW or WNW, are reverse faults; faults F2, F4, and F5, striking E-W or NE, are left-lateral strike-slip faults. Because of the heavy erosion and remote location, no convincing evidence was found to indicate the sense of motion of faults F6 and F7. A trench excavated in alluvial deposits across the major fault (F5) in the Ayouqi fault zone suggests that the most recent earthquake occurred between ca. 11.05 ± 0.52 ka and ca. 4.06 ± 0.29 ka.

F1

Two rows of anticlines (Fold 1 and Fold 2) of ~20 km length are present south of Ayouqi town (Fig. 6). The axis of Fold 1 bends from EW striking in the west portion to NW striking in the east, and the axis of Fold 2 has a NW trend. Geological mapping suggests that the Jurassic and Cretaceous sediments were folded and consistently dip to the southwestern direction (GBGMR, 1971) (Fig. 7a). Field investigations indicate that the late Quaternary alluvium covering these late Mesozoic sediments also has been offset by folding. Along the northeastern front of Fold 2, an active fault (F1) displaced alluvial-fan surfaces forming remarkable fault scarps (Figs. 7a, b). Several trenches excavated across the fault scarps reveal that the Jurassic deposits were thrust over late Quaternary conglomerates by reverse faulting (Figs. 7c-f). No strike-slip evidence was found along the fault trace. Synthesizing the dip of the Jurassic and Cretaceous sediments and the kinematics of F1, we infer a monocline deformation pattern to account for the surface observations of the two parallel anticlines and the associated thrusting without subsurface information or geodesy. (Fig. 7g). Under northeastward extrusion, the Jurassic and Cretaceous sediments may be compressed along a detachment at depth, which links the two folds and extends to the range front of Fold 2 to form the fault (F1) as seen at the surface. The deformation pattern also accounts for the folding along Fold 1 as the result of a ramp in depth (Fig. 7g).

F2

The fault F2 lies to the south of Ayouqi town, and extends ~5 km with an E-W strike (Fig. 7a). There is extensive coal mining along the fault trace, and most portions of the fault scarps have

been destroyed. To the west of province road S307, a north-facing fault scarp of ~1 km length is well preserved (Fig. 8a). The fault scarp is 1-4 m high without convincing evidence for strike slip based on geomorphological features. To determine the fault geometry in shallow surface, we excavated two trenches (Trench A and Trench B) across the fault scarp, separated by a distance of ~500 m (Fig. 8a). Strata revealed in these two trenches are similar (Figs. 8b, c). South of the main fault zone, units 1 and 2 are yellow lacustrine fine sandy silt. To the north, units 3 and 4 are late Quaternary fluvial or alluvial gravel and sand layers. Unit 5 is aeolian sand that blankets units 3 and 4 in Trench A. In Trench A, the main fault zone is marked by a ~1 m wide shear zone consisting of oriented clasts and elongated sandy silt along the fault plane (Fig. 8b). The main fault zone dips to the north at angle of ~80° with normal slip. Another fault in units 1 and 2 displaces the bottom of unit 2, showing no evidence for late Quaternary activity. In unit 3, several vents filled by fine sand are encountered in the trench exposure. Combining these opened vents and normal slip along the main fault zone suggests that Trench A experiences extension in the late Quaternary. In Trench B, the main fault zone is composed of three faults that merge near the base of the excavation and splay upward, showing a positive flower structure (Fig. 8c). The northernmost branch splays upward with a dip of 50°-70° to the south, juxtaposing units 1 and 2 over unit 3. It suggests a reverse component for the main fault zone in Trench B. Therefore, within the length of ~1 km, two trenches reveal both extensional and compressional motions along the main fault zone, suggesting that fault F2 may act as a strike-slip fault with a nearly vertical dip at depth. Considering the northeastward-thrusting fault F1 and the two folds (Fold 1 and Fold 2) to the south, we infer that F2 is a left-lateral strike-slip fault.

F3

The WNW trending fault F3 lies along the boundary between the bedrock and alluvium to the east of Ayouqi town (Fig. 7a). At the western end, the fault F3, dipping $\sim 40^\circ$ NEN, cuts a late Quaternary alluvial fan and juxtaposes Paleozoic granite over Jurassic sandstone (GBGMR, 1971) (Fig. 9a). The vertical displacement of the alluvial-fan surface is 5-7 m (Fig. 9b). Farther east, the fault trace runs along the southern flank of the range. Natural geological transects show that the fault plane dips 30° - 40° NEN with reverse motion (Figs. 9c, d). Absence of evidence for strike slip and the low-angle fault planes may suggest that fault F3 is a reverse fault in the late Quaternary.

F4

The ~ 6 km NE striking fault F4 lies in the inner mountain in the east of Ayouqi town (Fig. 6). Based on geomorphological expressions along the fault trace, F4 can be divided into two segments. The northeastern segment with length of ~ 3 km lies along a linear valley in bedrock. The southeastern segment has displaced two alluvial fans, forming clear fault scarps (Figs. 10a, b). On the older alluvial fan (Q_2) surface, the vertical displacement is 7-9 m and a series of gullies are offset by about 30-35 m with a sinistral sense (Fig. 10c). On the younger alluvial fan (Q_1), the surface is displaced less than 0.3 m vertically, and an offset stream shows a left-lateral strike slip of ~ 0.8 m (Fig. 10d). Alternately facing fault scarps (Fig. 10b) and apparent left-lateral strike slip relative to dip slip suggest that F4 is characterized as a left-lateral strike-slip fault.

F5

Fault F5, extending for ~30 km with an E-W strike, is the most extensive fault in the Ayouqi fault zone (Fig. 6). It is divided into two segments by a small inner-mountain basin (B2). The fault has experienced a nearly pure left-lateral movement along the southern margin of basins B1 and B3, cutting alluvial fans and displacing gullies. In the eastern segment, the fault appears as a relatively straight line on satellite imagery (Fig. 11a), indicative of a nearly vertical fault plane at depth. Several gullies have been displaced in a sinistral sense of motion with negligible vertical offset. To estimate the magnitude of the lateral displacement, we constructed orthoimages along parts of the fault trace using the SfM technique (Fig. 11b). The fault trace runs along the boundary between the granite and the alluvial fans that covered by thin alluvial sediments. Within ~1 km distance, 16 gullies were consistently displaced by ~3-5 m in left-lateral sense, as visible not only on the orthoimages (Figs. 11b-d), but also in the field (Fig. 11e). bedrock fault plane is exposed in a stream cutting parallel to the fault trace, showing an almost vertical dip (Fig. 11f). All these features clearly indicate that the fault F5 acts as a left-lateral strike-slip fault with no significant dip slip.

Along the western segment, fault F5 has displaced alluvial fans along the southern margin of basin B1, showing straight continuous fault scarps. Unlike the eastern segment, the western segment has a noticeable dip-slip component. Except for the present and most extensive alluvial fan Q_0 , three alluvial fans (Q_1 - Q_3) along this segment are displaced by the fault (Figs. 12a, b). The oldest alluvial fan (Q_3) is sporadically preserved along the fault trace. Fault scarps that displace this group of fans have heights of 6-7 m. Q_2 is more extensive with fault scarps in the range of 3-5 m high. Q_1 is slightly higher than the active channels and Q_0 . Fault scarps on Q_1 are

only ~20-30 cm high (Fig. 12c), which may result from the rupture of the most recent earthquake. To determine the timing of the earthquake that ruptured this young alluvial-fan surface, we dug a trench across the fault scarp as shown in Figs. 12a, d. The strata in the trench can be divided into four units (Figs. 12e, f). Unit 1 is white schist. Unit 2 is poorly sorted grey gravel layer in level mixed with fine sands. Unit 3 is similar to unit 2, but with larger gravels. Unit 4 is grey-white sandy silt representing floodplain deposition. The ~80° north dipping fault plane is marked by a ~30 cm shear zone between units 1 and 2, and covered by unit 3. This allows us to conclude that only one earthquake occurred with the dimensions of the trench, which postdates unit 2 and predates unit 3. Two OSL samples taken from the sandy layer in unit 2 and the sandy silt in unit 4 yield an age of 11.05 ± 0.52 ka and 4.06 ± 0.29 ka, respectively (Table 2). The faulted strata and OSL dating results suggest that the most recent earthquake on F5 occurred between ca. 11.05 ± 0.52 ka and ca. 4.06 ± 0.29 ka.

F6 and F7

The easternmost Ayouqi fault zone is composed of two active faults, F6 and F7 (Figs. 6 and 13). F6 extends for ~7 km with a NE strike, and with a scarp that is heavily eroded or covered by aeolian sands. The fault scarps are terminated near the boundary between the granite and the Jurassic deposits (Fig. 13). F7 extends for ~8 km and bends to the south along a bedrock-alluvial contact, more suggestive of dip slip. No detailed fieldwork has been conducted because of its remoteness. Roughly 35 km NE of F7, another important active fault, the Yabrai fault, lies in the inner Gobi Alashan block (Fig. 1b). Yu et al. (2016) suggest that the southwestern segment of the Yabrai fault, which trends NE, is a normal fault with a left-lateral strike-slip component,

whereas the northeastern segment is dominated by left-lateral strike slip. The Jurassic and Cretaceous sediments between the Ayouqi fault zone and the Yabrai fault are folded forming several alternatively distributed anticlines and synclines (Fig. 13). The boundary between the Jurassic and Cretaceous deposits is not offset in the geological map (Fig. 13). Meanwhile no fault scarp was found beyond the boundary between the Granite and Cretaceous deposits on the high-resolution satellite imagery and in field investigations. It suggests that the Ayouqi fault zone does not extend farther east and does not connect with the Yabrai fault.

6. Discussion

6.1 Geometry and kinematics of the Taohuala Shan-Ayouqi fault zone

The Taohuala Shan fault is about 30 km long and is characterized by left-lateral strike slip. It consists of three segments, i.e. western, step-over, and eastern segments. At the surface, the E-W trending western segment is concentrated on a single fault trace along most of the portions. Shutter ridges, offset streams, and hill-facing fault scarps suggest that this segment is a left-lateral strike-slip fault. An abrupt change in strike (10° - 15°) occurs with the step-over zone, which consists of many short sub-parallel fault splays within a width of ~1.5 km. The geometry of these fault splays in shallow surface indicates a positive flower structure. The eastern segment trends WNW and is a left-lateral strike-slip fault to the west of Site 6, whereas reverse motion dominates to the east. Thus, we conclude that the Taohuala Shan fault is a left-lateral strike-slip fault in the late Quaternary. At the easternmost end of the fault, lateral-strike slip is transferred into reverse component and folds along the fault trace.

The Ayouqi fault zone consists of seven active faults with different trends and slip motions. F1, approximately 20 km long, is developed along the range front of a fold (Fold 2) to the south of Ayouqi town. Remarkable surface fault scarps and fault geometry revealed in trenches and natural exposures, suggesting that F1 is characterized by northeastward thrusting. Two trenches excavated across F2 indicate different faulting motions, one is a high-angle normal fault and the other shows a positive flower structure, suggesting that F2 may be a strike-slip fault with nearly vertical dip at depth. Although no geomorphic evidence for lateral-strike slip was found along the fault trace, the NW-trending anticlines and associated reverse fault (F1) that developed to the south of F2, which suggest NE-directed shortening, also support that F2 may have a left-lateral strike-slip component. F3 trends NW and is sited to the east of Ayouqi town. Fault scarps preserved on alluvial-fan surfaces and low-angle thrusts exposed in natural transects indicate that F3 is a low-angle reverse fault in the late Quaternary. The NE-trending F4 extends for ~6 km in the mountain interior. Consistently displaced streams in sinistral sense, small vertical offset, and alternately facing fault scarps suggest that F4 is also a left-lateral strike-slip fault. As the major active fault in the Ayouqi fault zone, F5 is characterized as a nearly pure left-lateral strike-slip fault. A body of streams were offset along the fault trace without remarkable vertical displacement. We have no evidence for the kinematics of the two easternmost active faults, F6 and F7, because of the heavy erosion and remote location. The boundary between the Jurassic and Cretaceous deposits has not been displaced and no fault scarp in the late Quaternary alluviums is observed, suggesting that the Ayouqi fault zone has not linked with the Yabrai fault to the northeast.

Synthesizing the geometry and kinematics of all these active faults in the Taohuala Shan-Ayouqi fault zone, we can see that all the faults with an E-W trend are left-lateral strike-slip faults, and all the faults with a NW trend are reverse faults. These two groups of active faults with distinct kinematics and trending directions appear to be compatible with an overall regime that involves NE-directed shortening. The folding south of Ayouqi town and the left-lateral strike slip along the NE-trending fault F4 are also compatible with this regional shortening. This is supported by short-term GPS velocities, which indicate that the southern Gobi Alashan block is undergoing northeastward movement with respect to stable Eurasia (Gan et al., 2007).

The Taohuala Shan fault and the major fault (F5) in the Ayouqi fault zone are both ~30 km long. Given the lengths of these two faults, following standard earthquake scaling relationships (Scholz, 1982; Wells and Coppersmith, 1994), each fault would fail in earthquakes up to M_w 6.5, involving average slip of ~1.5 m. At the slip rate of 0.14-0.94 mm/yr determined along the Taohuala Shan fault, the repeat time of large earthquakes would be more than 1.6 ka. Notably, there is no record of M_w 6 earthquakes in the Taohuala Shan-Ayouqi fault zone and Ayouqi Town is located less than 1 km to the active fault trace, it poses a considerable hazard to local populations.

6.2 The role of the Taohuala Shan-Ayouqi fault zone in strain partitioning in the northeastern Tibetan Plateau

Field investigations and satellite imagery interpretations suggest that the Taohuala Shan-Ayouqi fault zone consists of several active faults whose lengths are less than ~30 km. These active

faults are characterized by left-lateral strike-slip or thrusting motion, which is compatible with regional NE-directed shortening. The left-lateral strike-slip rate is estimated to be <1 mm/yr in the late Quaternary. The strike slip along the two major active faults (the Taohuala Shan fault and F5 in the Ayouqi fault zone) is accommodated by reverse faulting and folding at the ends, so they do not connect with other active faults in the southern Gobi Alashan block.

The northeastern Tibetan Plateau, north of the Qaidam basin and south of the Hexi Corridor, is characterized by a series of WNW or NW trending ranges. These ranges all terminate at the Altyn Tagh fault, which is the longest active strike-slip fault within the Himalayan-Tibetan orogen and defines the northwestern margin of the northeastern Tibetan Plateau. Concerted effort over recent decades has led to estimate of ~ 10 mm/yr averaged over both Quaternary and decadal time scales (e.g., Shen et al., 2001; Zhang et al., 2004, 2007; Elliott et al., 2008; Cowgill et al., 2009; Gold et al., 2009, 2011). However, it remains controversial as to how the left-lateral strike slip along the Altyn Tagh fault is accommodated (Burchfiel et al., 1989; Meyer et al., 1998; Yin et al., 2002), especially for its eastern segment north to the Subei basin. Recently, with more and more studies on slip rates along the Altyn Tagh fault and WNW-thrusting faults that bound the elongated ranges in the northeastern Tibetan Plateau based on geological and geodetic estimations, it suggests that the total NEN-SWS convergence rate across the Qilian Shan matches the slip rate along the Altyn Tagh fault, which might indicate that the strike slip has been transferred into crustal shortening in the Qilian Shan (Zheng et al., 2013d; Zhang et al., 2016b; Liu et al., 2017). This is supported by progressive northeastward decreasing of the slip rate along the Altyn Tagh fault (Xu et al., 2005; Zhang et al., 2007; Zheng et al., 2013d). On the other hand, recent studies suggest that the active faults in the western Hexi Corridor are isolated reverse

faults (e.g., Zheng et al., 2013a, b; Zhang et al., 2016b), so the left-lateral strike slip along the Altyn Tagh fault may not extend into the Hexi Corridor and the southern Gobi Alashan in the late Quaternary. Although the Taohuala Shan-Ayouqi fault zone is characterized by left slip, we prefer to consider it as an oblique fault system to accommodate regional NE-directed shortening, but not the northeastward extension of the Altyn Tagh fault.

Yu et al. (2016) suggest the southwestern and middle segments of the Yabrai fault, which is the most outstanding fault in the inner Gobi Alashan block, appear to exhibit oblique-normal displacement with a minor sinistral component, whereas the northeastern segment is primarily sinistral strike-slip with a minor reverse component. Based on field investigations on the geometry and slip motions along different segments of the Yabrai fault and limited satellite imagery interpretations on the Taohuala Shan-Ayouqi fault zone, they proposed a northeastward oblique extrusion model for the southern Gobi Alashan. In the deformation model of the southern Gobi Alashan block that proposed by Yu et al. (2016), the northeastern segment of the Yabrai fault and the Taohuala Shan-Ayouqi fault zone represent strike-slip faults bounding a left step in a sinistral system, and the southeastern and middle segments of the Yabrai fault lies in a release bend zone that is dominated by normal faulting. Our field investigations in this study have affirmed that the Taohuala Shan-Ayouqi fault zone is characterized by left-lateral strike slip. On the other hand, the slip rate along the northeastern segment of the Yabrai fault is estimated to be 0.2-0.7 mm/yr (Yu et al., 2016), which is in agreement with the slip rate along the Taohuala Shan-Ayouqi fault zone (0.14-0.93 mm/yr). It might suggest that the southern Gobi Alashan acts as a rigid block in the late Quaternary.

6.3 Implications for active tectonics in the Hexi Corridor and southern Gobi Alashan

The Hexi Corridor is a narrow foreland basin associated with the NE-directed thrusting of the northern Tibetan Plateau (Tapponnier et al., 2001; Zheng et al., 2017) (Fig. 1a). It lies in the transitional zone between northern Tibet and the Gobi Alashan block. As mentioned above, two scenarios have been put forward to explain the active faulting in the Hexi Corridor. One is that the Hexi Corridor is considered as a wedge-top depozone within an idealized foreland basin system bounded by thrust faults to the north (Bovet et al., 2009; Zheng et al., 2013a). The other one suggests that most of the active faults in the Hexi Corridor are left-lateral strike-slip faults that link with the northeastward extension of the Altyn Tagh fault (Yue and Liou, 1999; Darby et al., 2005; Chen and Xu, 2006). Here, we present both left-lateral strike-slip faults and reverse faults in the Taohuala Shan-Ayouqi fault zone in the southern Gobi Alashan. The localized geometry and kinematics of the Taohuala Shan-Ayouqi fault zone provides insight into understanding the deformation pattern for the entire Hexi Corridor.

A few studies of the active faults in the Hexi Corridor have been published. Hetzel et al. (2002) estimate slip rates of 0.35 mm/yr for the Yumen fault (YMF), which is a thrust fault that trends in WNW striking north of Yumen city (Fig. 14a). Combining satellite imagery analysis, topographic profiling with OSL and ^{10}Be exposure dating, Zheng et al. (2013b) suggest that the NW trending Jiayuguan fault (JYGF) is a reverse fault with vertical slip rate of ~ 0.22 mm/yr. Another two NW-trending active faults in the western Hexi Corridor, the Xinminpu fault (XMBF) and the Yinwa Shan fault (YWSF), are also reverse faults (Min et al., 2002; Zheng et al., 2013b). The Hei Shan fault (HSF) strikes E-W and is a high-angle reverse fault as revealed by natural

exposures (Zheng, 2009; Zhang et al., 2016b). To the east, the Jinta Nan Shan fault (JNSF) that trends N100° is a high-angle reverse fault with a left-lateral strike-slip component (Zheng, 2009; Zhang et al., 2016a), although Zheng et al. (2013b) considered this strike slip as the effect of asymmetric topography. The southern Heli Shan fault (HLSF), the boundary between the Hexi Corridor and the Gobi Alashan block, is a reverse fault with no strike slip in the late Quaternary based on the displacement measurements along the fault trace (Hetzl et al., 2004; Zheng et al., 2013a). East of the Heli Shan, the E-W trending Beida Shan fault (BDSF), which is characterized as several relatively straight lines on satellite imagery, was considered as a left-lateral strike-slip fault based on analysis of geological maps and satellite imagery and sparse evidence from field investigations (Darby et al., 2005; Chen and Xu, 2006). In the field, we also found that some streams and terrace risers are offset with a sinistral sense of motion, and the vertical displacement across fault traces is negligible at some sites. Although much more detailed fieldwork is needed to identify the kinematics of the Beida Shan fault, we prefer to regard it as a left-lateral strike-slip fault with a reverse component. Farther east, in the southern Gobi Alashan, our results suggest that the Taohuala Shan fault (TSF) is a left-lateral strike-slip fault, and the faults in the Ayouqi fault zone are either strike-slip faults or reverse faults depending on their strikes. To the south of the Taohuala Shan-Ayouqi fault zone, the Longshou Shan that is parallel to the Qilian Shan is the most remarkable mountain in the Hexi Corridor. Both the southern and northern range flank are bounded by reverse faults (Meyer et al., 1998; Palumbo et al., 2010). At the eastern end of the Longshou Shan, an E-W trending active fault, which we name the Jinchang fault (JCF), is considered as the source of the 1956 Ms 7.0 Minqin earthquake (Liu et al., 2000). Striae observed on fault planes indicate that the fault has left-lateral strike-slip and reverse components (Liu et al., 2000).

Among these active faults in the Hexi Corridor, all the active faults that trend in E-W striking (except for the Hei Shan fault) are left-lateral strike-slip faults or with a sinistral component, such as the Jinta Nan Shan, Beida Shan, Taohuala Shan, Jinchang faults, and faults F2 and F5 in the Ayouqi fault zone (Fig. 14a). Whereas all the active faults that trend in NW or WNW striking are reverse faults, such as the Yumen, Xinminbu, Yinwa Shan, Jiayuguan, southern Heli Shan, northern and southern Longshou Shan faults, and faults F1 and F3 in the Ayouqi fault zone. Thus, we conclude that the active faults in the Hexi Corridor and the southern Gobi Alashan are neither all left-lateral strike-slip faults that were considered as the northeastward extension of the Altyn Tagh fault (Darby et al., 2005; Chen and Xu, 2005), nor all reverse faults that are splays of a decollement at depth linked with the northeastward extrusion of northern Tibet (Tapponnier et al., 2001; Zheng et al., 2013a). We propose an oblique-extrusion deformation model for the Hexi Corridor and the southern Gobi Alashan in the late Quaternary (Fig. 14b). All the left-lateral strike-slip and reverse faults in this area are compatible with the NE-directed shortening. When the faults strike perpendicular to the shortening direction, they are reverse faults. Whereas when the faults trend in E-W direction, they are left-lateral strike-slip faults. With less than 100 km from the active faults in the Hexi Corridor and southern Gobi Alashan to the northern margin of the Qilian Shan, which is dominated by northeast-verging thrusts, the NE-directed shortening is apparently associated with the northeastward extrusion of the northern Tibetan Plateau.

7. Conclusions

Based on the field investigations and high-resolution imagery interpretations, we conclude that the Taohuala Shan fault is a left-lateral strike-slip fault in the late Quaternary. It consists of three segments, western, step-over, and eastern segments. Combining topographic surveys with dating of the alluvial surfaces suggests a left-lateral strike-slip rate of 0.14-0.93 mm/yr, and a vertical slip rate of 0.1-0.3 mm/yr. The Ayouqi fault zone is composed of seven faults with different strikes and senses of motion. Among them, the faults (F1 and F3) trending NW or WNW are reverse faults, whereas the faults (F2 and F5) trending E-W are left-lateral strike-slip faults, which are compatible with regional NE-directed shortening. The last event that ruptured the major fault, F5, in the Ayouqi fault zone occurred between ca. 11.05 ± 0.52 ka and ca. 4.06 ± 0.29 ka. Synthesizing of the geometry and kinematics of most active faults in the Hexi Corridor and the southern Gobi Alashan, suggests that this region experiences NE-directed shortening associated with the northeastward extrusion of the northern Tibetan Plateau in the late Quaternary. Therefore, the active faults striking parallel to the Qilian Shan are all reverse faults, and those with E-W trend are left-lateral strike-slip faults because of oblique compression. The faults do not link with the Altyn Tagh fault and do not form a NE continuation of the Altyn Tagh fault.

Acknowledgments

This research was funded by the National Science Foundation of China (41372220, 41590861, 41661134011), Public Service Funds for Earthquake Studies (201408023), and the Strategic Priority Research Program of the Chinese Academy of Sciences (XDB03020201). We thank Li Zhang for her helps in processing dating samples and Yu Zhou for his reviews on the language. Richard T. Walker is gratefully appreciated for his helpful discussions and detailed review on the language. We acknowledge An Yin and an anonymous reviewer for their positive and constructive reviews to improve this manuscript.

References

- Balco, G., Stone, J.O., Lifton, N.A., Dunai, T.J., 2008. A complete and easily accessible means of calculating surface exposure ages or erosion rates from ^{10}Be and ^{26}Al measurements. *Quaternary geochronology* 3, 174-195.
- Bonilla, M.G., Lienkaemper, J.J., 1991. Factors affecting the recognition of faults exposed in exploratory trenches. USGPO; For sale by the Books and Open-File Reports Section, US Geological Survey Bulletin 1947, 54.
- Bovet, P.M., Ritts, B.D., Gehrels, G., Abbink, A.O., Darby, B., Hourigan, J., 2009. Evidence of Miocene crustal shortening in the north Qilian Shan from Cenozoic stratigraphy of the western Hexi Corridor, Gansu Province, China. *American Journal of Science* 309, 290-329.
- Burbank, D.W., Anderson, R.S., 2012. *Tectonic geomorphology*. John Wiley & Sons, 92-104.
- Burchfiel, B., Deng, Q.D., Molnar, P., Royden, L., Wang, Y.P., Zhang, P.Z., Zhang, W.Q., 1989. Intracrustal detachment within zones of continental deformation. *Geology* 17, 748-752.
- Bureau of Geology and Mineral Resources of Gansu Province, 1989. *Regional Geology Gansu Province: Geological Memoirs Series 1, Volume 19*. Geological Publishing House, Beijing.
- Chen, W.B., Xu, X.W., 2006. Sinistral strike-slip faults along the southern Alashan margin and eastwards extending of the Altun fault. *Seismology and Geology* 28, 319-324 (in Chinese with English abstract).
- Cowgill, E., Gold, R.D., Chen, X.H., Wang, X.F., Arrowsmith, J.R., Southon, J., 2009. Low Quaternary slip rate reconciles geodetic and geologic rates along the Altyn Tagh fault, northwestern Tibet. *Geology* 37 (7), 647-650. doi: 10.1130/G25623A.1.
- Darby, B.J., Ritts, B.D., Yue, Y., Meng, Q., 2005. Did the Altyn Tagh fault extend beyond the Tibetan Plateau? *Earth and Planetary Science Letters* 240, 425-435.
- Elliott, J.R., Biggs, J., Parsons, B., Wright, T.J., 2008. InSAR slip rate determinations on the Altyn Tagh Fault, northern Tibet, in the presence of topographically correlated atmospheric delays. *Geophysical Research Letters* 35, L12309. doi: 10.1029/2008GL033659.
- Gan, W.J., Zhang, P.Z., Shen, Z.K., Niu, Z.J., Wang, M., Wan, Y.G., Zhou, D.M., Cheng, J., 2007. Present-day crustal motion within the Tibetan Plateau inferred from GPS measurements. *Journal of Geophysical Research: Solid Earth* 112 (B8), B08416. doi: 10.1029/2005JB004120.
- Gansu Bureau of Geological and Mineral Resources, 1971. *Geological map of the Shandan area, scale 1:200,000*. Geological Press, Beijing.
- Gold, R.D., Cowgill, E., Arrowsmith, J.R., Gosse, J., Chen, X., Wang, X.F., 2009. Riser diachroneity, lateral erosion, and uncertainty in rates of strike-slip faulting: A case study from Tuzidun along the Altyn Tagh fault, NW China. *Journal of Geophysical Research: Solid Earth* 114 (B4), B04401. doi: 10.1029/2008JB005913.
- Gold, R.D., Cowgill, E., Arrowsmith, J.R., Chen, X., Sharp, W.D., Cooper, K.M., Wang, X.F., 2011. Faulted terrace risers place new constraints on the late Quaternary slip rate for the central Altyn Tagh fault, northwest Tibet. *Geological Society of America Bulletin* 123 (5-6): 958-978. doi: 10.1130/B30207.1.
- Hanks, T.C., 2000. The age of scarplike landforms from diffusion-equation analysis. *Quaternary Geochronology: Methods and Applications*, 313-338.
- Hetzel, R., Niedermann, S., Tao, M., Kubik, P.W., Ivy-Ochs, S., Gao, B., Strecker, M.R., 2002. Low slip rates and long-term preservation of geomorphic features in Central Asia. *Nature* 417, 428-432.
- Hetzel, R., Tao, M., Niedermann, S., Strecker, M.R., Ivy-Ochs, S., Kubik, P.W., Gao, B., 2004. Implications of the fault scaling law for the growth of topography: Mountain ranges in the broken foreland of north-east Tibet. *Terra Nova* 16, 157-162.
- Johnson, K., Nissen, E., Saripalli, S., Arrowsmith, J.R., McGarey, P., Scharer, K., Williams, P., Blisniuk, K., 2014. Rapid mapping of ultrafine fault zone topography with structure from motion. *Geosphere* 10, 969-986.
- Kimura, G., Tamaki, K., 1990. Mesozoic collision-Extrusion tectonics in eastern Asia. *Tectonophysics* 5 (3), 389-401.
- Kohl, C., Nishiizumi, K., 1992. Chemical isolation of quartz for measurement of in-situ-produced cosmogenic nuclides. *Geochimica et Cosmochimica Acta* 56, 3583-3587.
- Lal, D., 1991. Cosmic ray labeling of erosion surfaces: in situ nuclide production rates and erosion models. *Earth and Planetary Science Letters* 104, 424-439.

- Liu, H.C., Dai, H.G., Li, L.H., Jia, Y.H., Yang, R., 2000. A preliminary study on the 1954 Minqin Ms 7.0 earth-quake in Gansu Province. *Northwestern Seismological Journal* 22, 232-235 (in Chinese with English abstract).
- Liu, X.W., Yuan, D.Y., Su, Q., 2017. Late Pleistocene slip rate of the northern Qilian Shan frontal thrust, western Hexi Corridor, China. *Terra Nova* 29, 238-244. doi: 10.1111/ter.12270.
- Lu, Y.C., Wang, X.L., Wintle, A.G., 2007. A new OSL chronology for dust accumulation in the last 130,000 yr for the Chinese Loess Plateau. *Quaternary Research* 67, 152-160.
- McCalpin, J.P., 2009. *Paleoseismology*. Academic press, 186-203.
- Meng, Q.R., 2003. What drove late Mesozoic extension of the northern China-Mongolia tract? *Tectonophysics* 369(3), 155-174.
- Meyer, B., Tapponnier, P., Bourjot, L., Metivier, F., Gaudemer, Y., Peltzer, G., Shunmin, G., Zhitai, C., 1998. Crustal thickening in Gansu-Qinghai, lithospheric mantle subduction, and oblique, strike-slip controlled growth of the Tibet plateau. *Geophysical Journal International* 135, 1-47.
- Min, W., Zhang, P.Z., He, W.G., Li, C.Y., Mao, F.Y., Zhang, S.P., 2002. Research on the active faults and paleoearthquakes in the western Jiuquan basin: *Seismology and Geology* 24, 35-44 (in Chinese with English abstract).
- Murray, A.S., Wintle, A.G., 2000. Luminescence dating of quartz using an improved single-aliquot regenerative-dose protocol. *Radiation measurements* 32, 57-73.
- Palumbo, L., Hetzel, R., Tao, M., Li, X., 2010. Topographic and lithologic control on catchment-wide denudation rates derived from cosmogenic ^{10}Be in two mountain ranges at the margin of NE Tibet. *Geomorphology* 117, 130-142.
- Tapponnier, P., Meyer, B., Avouac, J.P., Peltzer, G., Gaudemer, Y., Shunmin, G., Hongfa, X., Kelun, Y., Zhitai, C., Shuohua, C., 1990. Active thrusting and folding in the Qilian Shan, and decoupling between upper crust and mantle in northeastern Tibet. *Earth and Planetary Science Letters* 97, 382387-383403.
- Scholz, C.H., 1982. Scaling relations for strong ground motion in large earthquakes. *Bulletin of the Seismological Society of America* 72 (6), 1903-1909.
- Shen, Z.K., Wang, M., Li, Y., Jackson, D.D., Yin, A., Dong, D., Fang, P., 2001. Crustal deformation along the Altyn Tagh fault system, western China, from GPS. *Journal of Geophysical Research* 106, 30607-30621. doi: 10.1029/2001JB000349.
- Tapponnier, P., Molnar, P., 1977. Active faulting and tectonics in China. *Journal of Geophysical Research* 82, 2905-2930.
- Tapponnier, P., Zhiqin, X., Roger, F., Meyer, B., Arnaud, N., Wittlinger, G., Jingsui, Y., 2001. Oblique stepwise rise and growth of the Tibet Plateau. *Science* 294, 1671-1677.
- Thompson, S.C., Weldon, R.J., Rubin, C.M., Abdrakhmatov, K., Molnar, P., Berger, G.W., 2002. Late Quaternary slip rates across the central Tien Shan, Kyrgyzstan, central Asia. *Journal of Geophysical Research: Solid Earth* 107.
- Vincent, S.J., Allen, M.B., 1999. Evolution of the Minle and Chaoshui Basins, China: Implications for Mesozoic strike-slip basin formation in Central Asia. *Geological Society of America Bulletin* 111, 725-742.
- Webb, L., Johnson, C., 2006. Tertiary strike-slip faulting in southeastern Mongolia and implications for Asian tectonics. *Earth and Planetary Science Letters* 241, 323-335.
- Well, D.L., Coppersmith, K.J., 1994. New empirical relationships among magnitude, rupture length, rupture width, rupture area, and surface displacement. *Bulletin of Seismological Society of America* 84, 974-1002.
- Xu, X.W., Wang, F., Zheng, R.Z., Chen, W.B., Ma, W.T., Yu, G.H., Chen, G.H., Tapponnier, P., Van Der Woerd, J., Meriaux, A.S., Ryerson, F.J., 2005. Late Quaternary sinistral slip rate along the Altyn Tagh fault and its structural transformational model. *Science in China, Series D: Earth Sciences* 48, 384-397.
- Xu, X.W., Yeats, R.S., Yu, G.H., 2010. Five short historical earthquake surface ruptures near the Silk Road, Gansu Province, China. *Bulletin of the Seismological Society of America* 100, 541-561.
- Yin, A., Harrison, T.M., 2000. Geologic evolution of the Himalayan-Tibetan orogen. *Annual Review of Earth and Planetary Sciences* 28, 211-280.
- Yin, A., Rumelhart, P., Butler, R., Cowgill, E., Harrison, T., Foster, D., Ingersoll, R., Qing, Z., Xian-Qiang, Z., Xiao-Feng, W., 2002. Tectonic history of the Altyn Tagh fault system in northern Tibet inferred from Cenozoic sedimentation. *Geological Society of America Bulletin* 114, 1257-1295.

- Yu, J.X., Zheng, W.J., Kirby, E., Zhang, P.Z., Lei, Q.Y., Ge, W.P., Wang, W.T., Li, X.N., Zhang, N., 2016. Kinematics of late Quaternary slip along the Yabrai fault: Implications for Cenozoic tectonics across the Gobi Alashan block, China. *Lithosphere* 8, 199-218.
- Yuan, D.Y., Ge, W.P., Chen, Z.W., Li, C.Y., Wang, Z.C., Zhang, H.P., Zhang, P.Z., Zheng, D.W., Zheng, W.J., Craddock, W.H., 2013. The growth of northeastern Tibet and its relevance to large-scale continental geodynamics: A review of recent studies. *Tectonics* 32, 1358-1370.
- Yue, Y., Liou, J.G., 1999. Two-stage evolution model for the Altyn Tagh fault, China. *Geology* 27, 227-230.
- Zhang, P.Z., Molnar, P., Xu, X., 2007. Late Quaternary and present-day rates of slip along the Altyn Tagh Fault, northern margin of the Tibetan Plateau. *Tectonics* 26.
- Zhang, B., He, W.G., Pang, W., Wu, Z., Shao, Y.X., Yuan, D.Y., 2016a. Geological and geomorphic expressions of late Quaternary strike-slip activity on Jinta Nanshan fault in northern edge of Qing-Zang block. *Seismology and Geology* 38, 1-21 (in Chinese with English abstract).
- Zhang, N., Zheng, W.J., Liu, X.W., Wang, W.T., Li, X.N., He, W.G., Lei, Q.Y., Shao, Y.X., 2016b. Kinematics characteristics of Heishan fault in the western Hexi Corridor and its implications for regional tectonic transformation. *Journal of Earth Sciences and Environment* 38, 245-257 (in Chinese with English abstract).
- Zheng, D.W., Wang, W.T., Wan, J.L., Yuan, D.Y., Liu, C.R., Zheng, W.J., Zhang, H.P., Pang, J.Z., Zhang, P.Z., 2017. Progressive northward growth of the northern Qilian Shan–Hexi Corridor (northeastern Tibet) during the Cenozoic. *Lithosphere*, L587. 581.
- Zheng, W.J., 2009. Geometry pattern and active tectonics of the Hexi Corridor and its adjacent regions. Ph.D Thesis, Institute of Geology, China Earthquake Administration (in Chinese with English abstract).
- Zheng, W.J., Zhang, P.Z., Ge, W.P., Molnar, P., Zhang, H.P., Yuan, D.Y., Liu, J.H., 2013a. Late Quaternary slip rate of the South Heli Shan Fault (northern Hexi Corridor, NW China) and its implications for northeastward growth of the Tibetan Plateau. *Tectonics* 32, 271-293.
- Zheng, W.J., Zhang, H.P., Zhang, P.Z., Molnar, P., Liu, X.W., Yuan, D.Y., 2013b. Late Quaternary slip rates of the thrust faults in western Hexi Corridor (Northern Qilian Shan, China) and their implications for northeastward growth of the Tibetan Plateau. *Geosphere* 9, 342-354.
- Zheng, W.J., Zhang, Z.Q., Zhang, P.Z., Liu, X.W., Guo, X., Pang, J.Z., Ge, W.P., Yu, J.X., 2013c. Seismogenic structure and mechanism of the 1954 M7.1/4 Shandan Earthquake, Gansu Province, Western China. *Chinese Journal of Geophysics* 56, 916-928 (in Chinese with English abstract).
- Zheng, W.J., Zhang, P.Z., He, W.G., Yuan, D.Y., Shao, Y.X., Zheng, D.W., Ge, W.P., Min, W., 2013d. Transformation of displacement between strike-slip and crustal shortening in the northern margin of the Tibetan Plateau: Evidence from decadal GPS measurements and late Quaternary slip rates on faults. *Tectonophysics* 584, 267-280.
- Zhou, Y., Parsons, B., Elliott, J., Barisin, I., Walker, R., 2015. Assessing the ability of Pleiades stereo imagery to determine height changes in earthquakes: A case study for the EI Mayor-Cucapah. *Journal of Geophysical Research: Solid Earth* 120, 8793-8808.
- Zorin, Y.A., Belichenko, V., Turutanov, E.K., Mazukabzov, A., Sklyarov, E., Mordvinova, V., 1995. The east Siberia transect. *International Geology Review* 37 (2), 154-175.

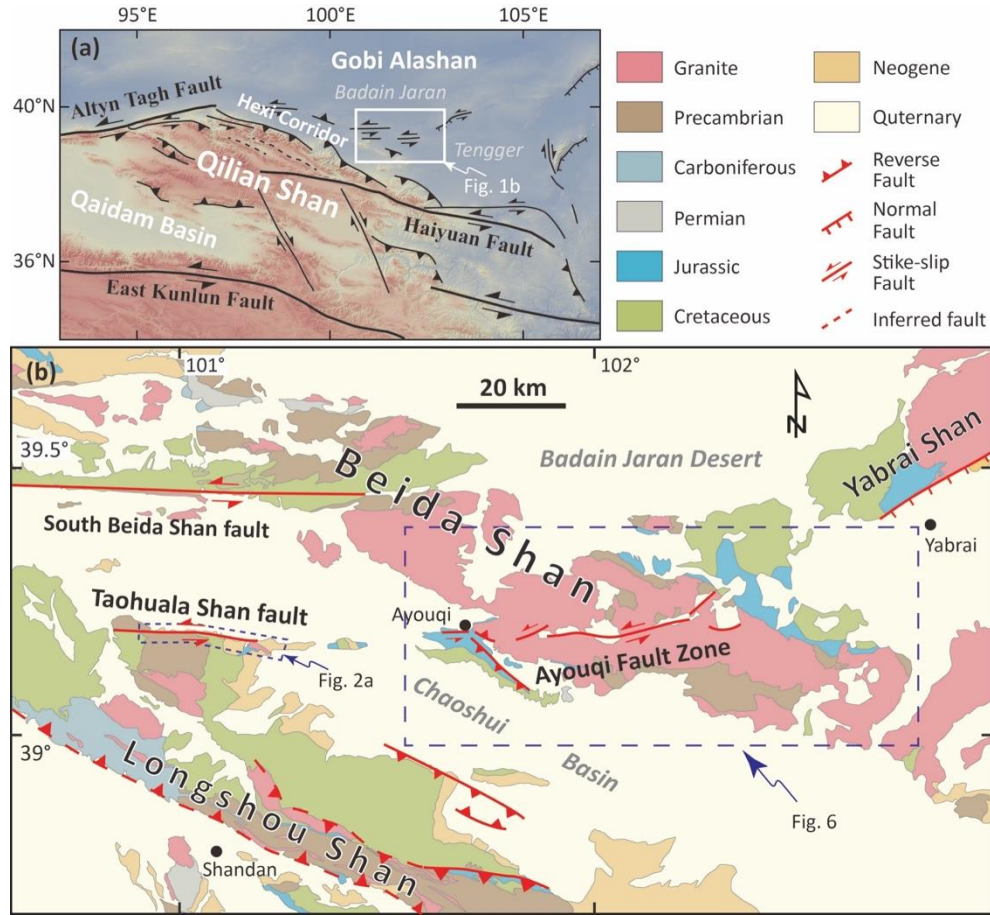
Figure 1

Fig. 1. (a) Topographic map of the northeastern margin of the Tibetan Plateau showing major active faults and the location of the study area. Active faults are modified after Yuan et al. (2013) and Zheng et al. (2013a); (b) Geological overview map of the study area, showing geological rock units and active faults. Distribution of deposits compiled from GBGMR (1989). The geometry of active faults is from our field investigations and Yu et al. (2016).

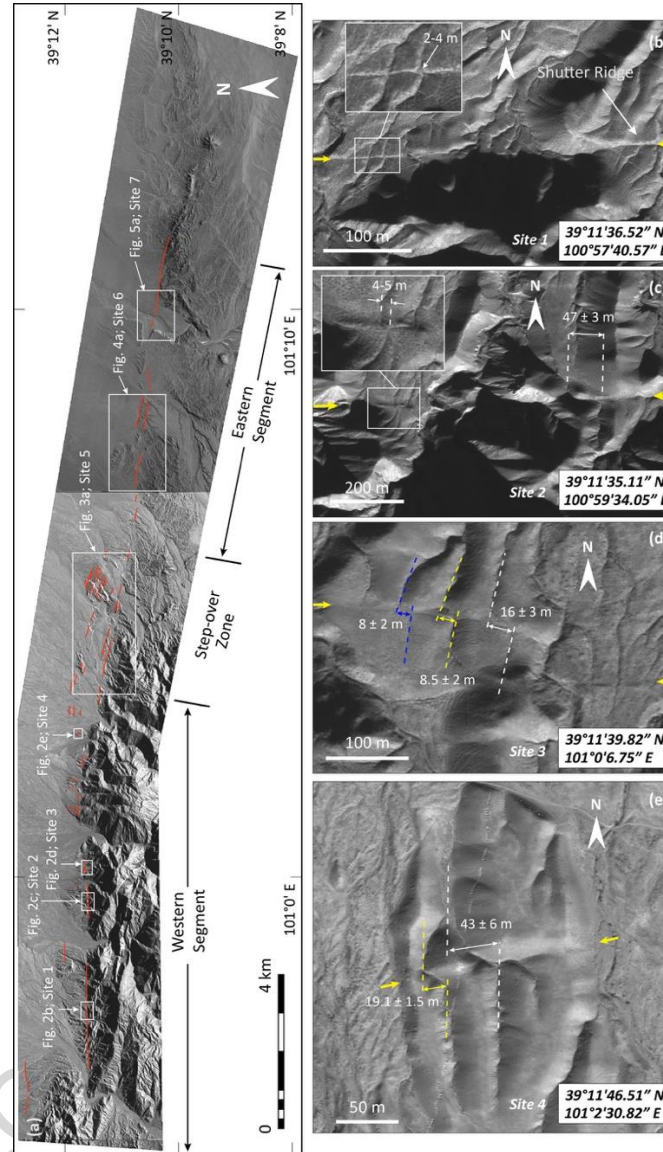
Figure 2

Fig. 2. Geomorphological features along the Taohuala Shan fault shown on WorldView satellite imagery. Red lines refer to the locations of fault scarps. (a) WorldView satellite image with resolution of 0.5 m shows the active fault trace and the locations of work sites. Location is shown in Fig. 1b; (b) Site 1 shows a fault trace displaced alluvial fans. The inset shows a stream developed on lower alluvial-fan surface that is offset by 2-4 m in a sinistral sense of motion. Higher alluvium is displaced forming a shutter ridge that blocks northward flowing streams. Yellow arrows indicate the location of the fault trace; (c) Site 2. The Inset shows a pressure ridge developed along the fault trace, with a stream across the fault displaced by 4-5 m by lateral slip. An incised gully is displaced by 47 ± 3 m in sinistral sense; (d) Site 3 shows two strands of fault scarps. Along the northern one, three streams were displaced in sinistral sense by 8 ± 2 m, 8.5 ± 2 m, 16 ± 3 m; (e) Site 4 shows a relict alluvium cut by the fault. Two streams were offset by 19.1 ± 1.5 m, 43 ± 6 m, whereas the vertical displacement is only 1-3 m.

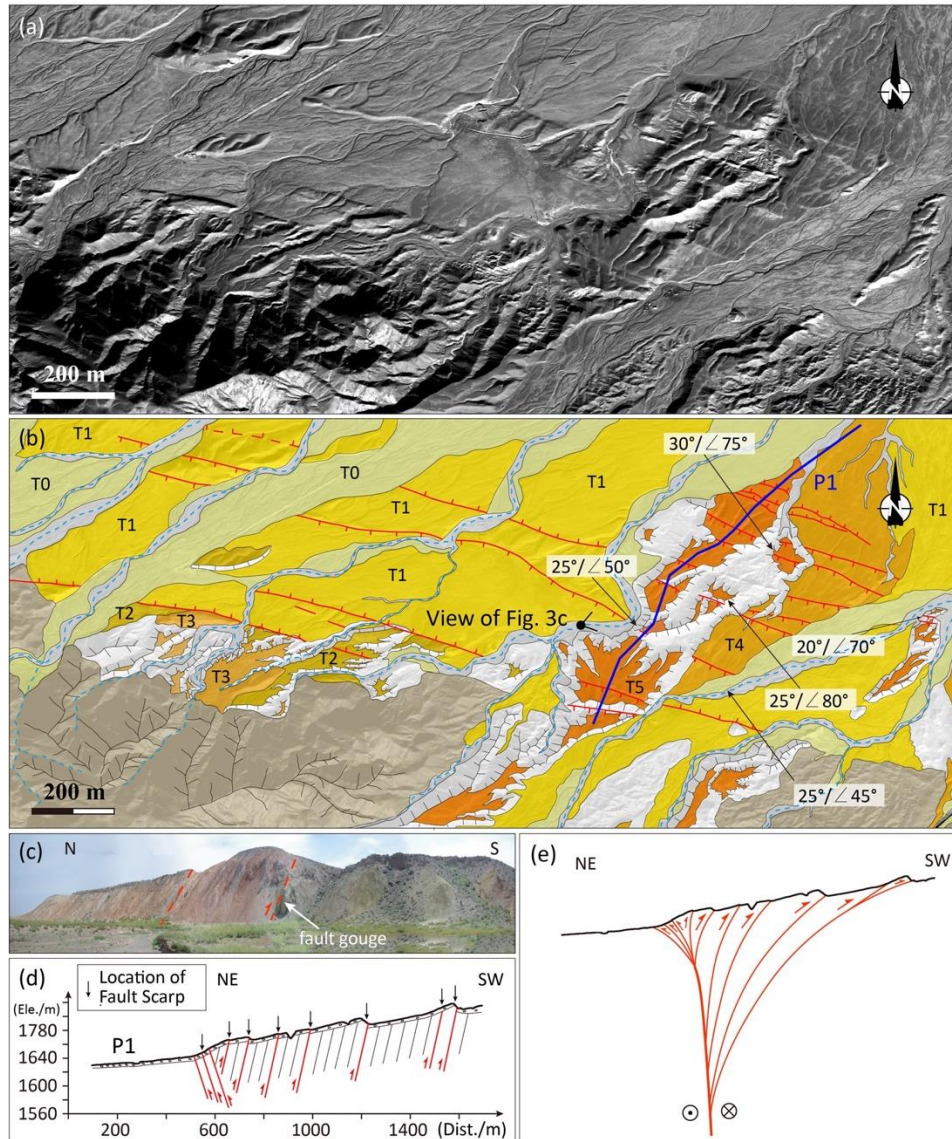
Figure 3

Fig. 3. (a) WorldView satellite image of the step-over zone in the Taohuala Shan fault, with resolution of 0.5 m. See Fig. 2a for location; (b) Interpretive map of the view of Fig. 3a. Red lines show the fault trace and ticks indicate dips of fault scarps. Six alluvial fans are mapped in this area, T0 is the active fan, and T5 is the highest and oldest fan. Blue line P1 indicates the location of the topographic profile in Fig. 3d. Dip directions and dip angles of bedding underneath the T4 and T5 fans are shown on the map; (c) Photograph showing a natural exposure with fault gouge under the fault scarps and northeast-dipping bedding. See location in Fig. 3b; (d) A geological transect along the natural exposure in the alluvial fan F5 based on field investigations. Seven fault scarps face south and the northmost three face north. Fault planes revealed by fault gouge are parallel to sedimentary bedding; (e) An inferred positive flower structure at depth underneath F5 based the geological transect in Fig. 3d.

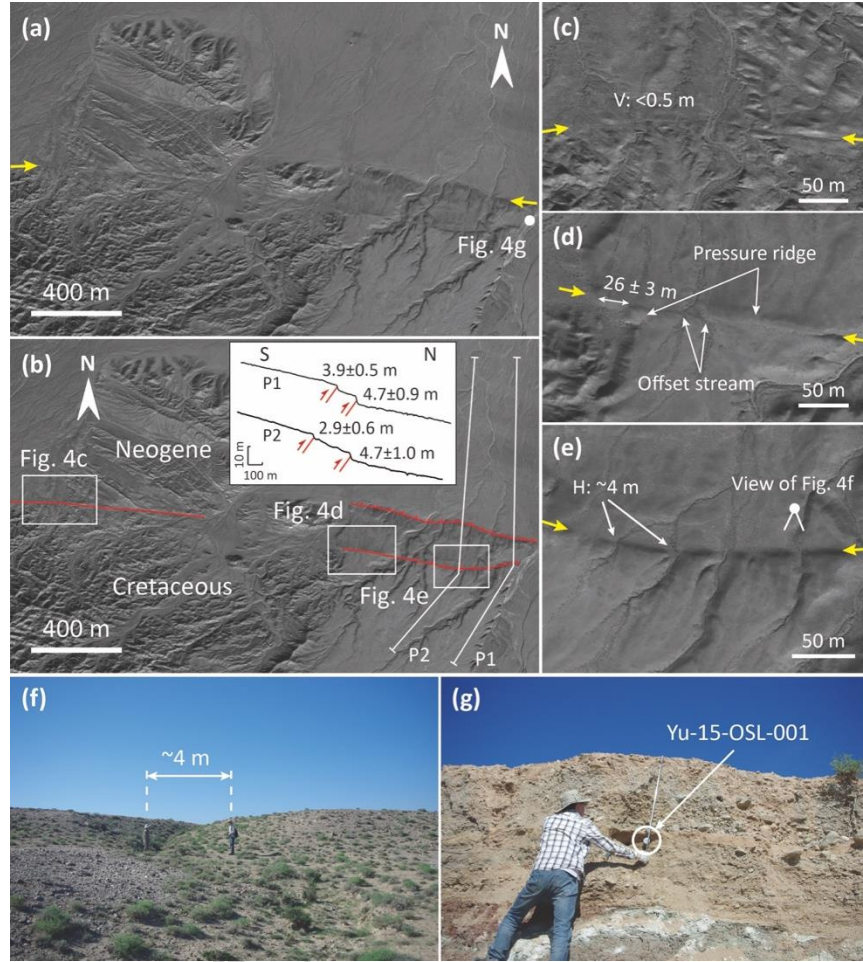
Figure 4

Fig. 4. (a) and (b) WorldView satellite image at Site 6. Red lines and yellow arrows show the locations of fault scarps. Inset in (b) shows topographic profiles showing vertical offsets on alluvium. Profile locations are marked in Fig. 4b; (c) Fault scarp with height of <0.5 m in the west of Site 6. “V” refers to vertical displacement. See location in Fig. 4b; (d) A pressure ridge developed along the fault trace, and streams and the riser of alluvial fan are displaced. See location in Fig. 4b; (e) Fault scarps on alluvial-fan surfaces. Several small streams were offset by about 4 m in left-lateral sense. “H” refers to horizontal displacement. See location in Fig. 4b; (f) Photograph showing a stream offset by ~4 m in sinistral sense. See location in Fig. 4e; (g) The OSL sample Yu-15-OSL-001 were collected from a lens of sand silt in the alluvial deposit. See sampling location in Fig. 4a.

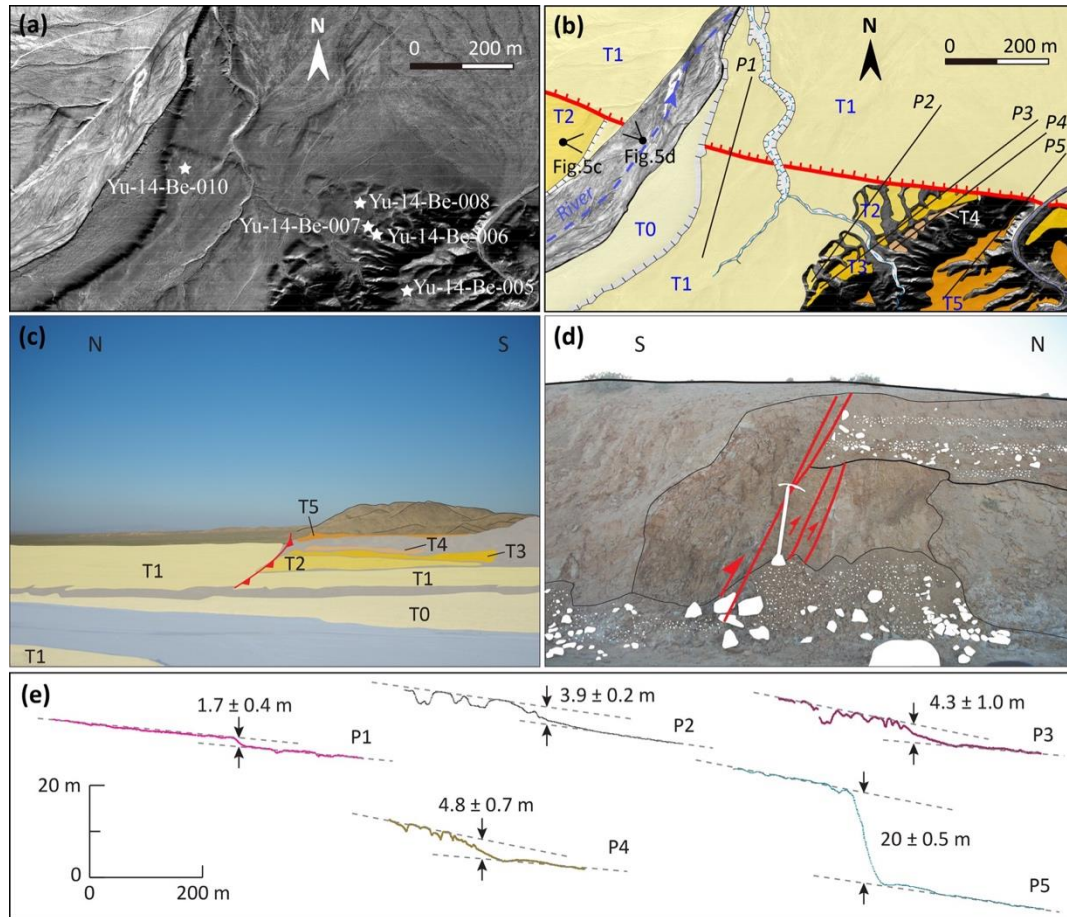
Figure 5

Fig. 5. (a) WorldView satellite image of Site 7. Stars show the locations of cosmogenic exposure age samples. See location in Fig. 2a; (b) Interpretive map of Fig. 5a. Red lines show location of fault scarps and ticks indicate dips of fault scarps. Five alluvial fans were preserved at this site. T0 is the floodplain and T5 is the highest relict alluvial surface. Lines labelled P1 to P5 show the locations of topographic profiles across the fault scarp; (c) Interpretive photograph showing the distribution of alluvial fans; (d) Fault exposure in the alluvial fan T1 on the western bank of the river, showing several branches of reverse faults. See location in Fig. 5b; (e) Topographic profiles of offset alluvial-fan surfaces. See location in Fig. 5b.

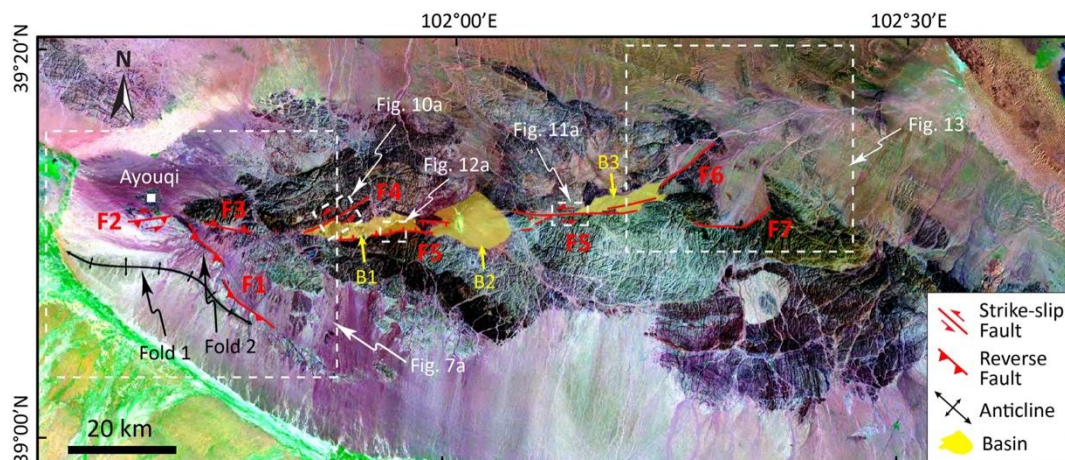
Figure 6

Fig. 6. Landsat ETM+ imagery of the Ayouqi fault zone. See location in Fig. 1b. Red lines show the locations of seven active faults that are labelled as F1 to F7. Ticks indicate dips of fault scarps. Two rows of anticlines, Fold 1 and Fold 2, are developed to south of Ayouqi town. Yellow polygons indicate three intermountane basins.

Figure 7

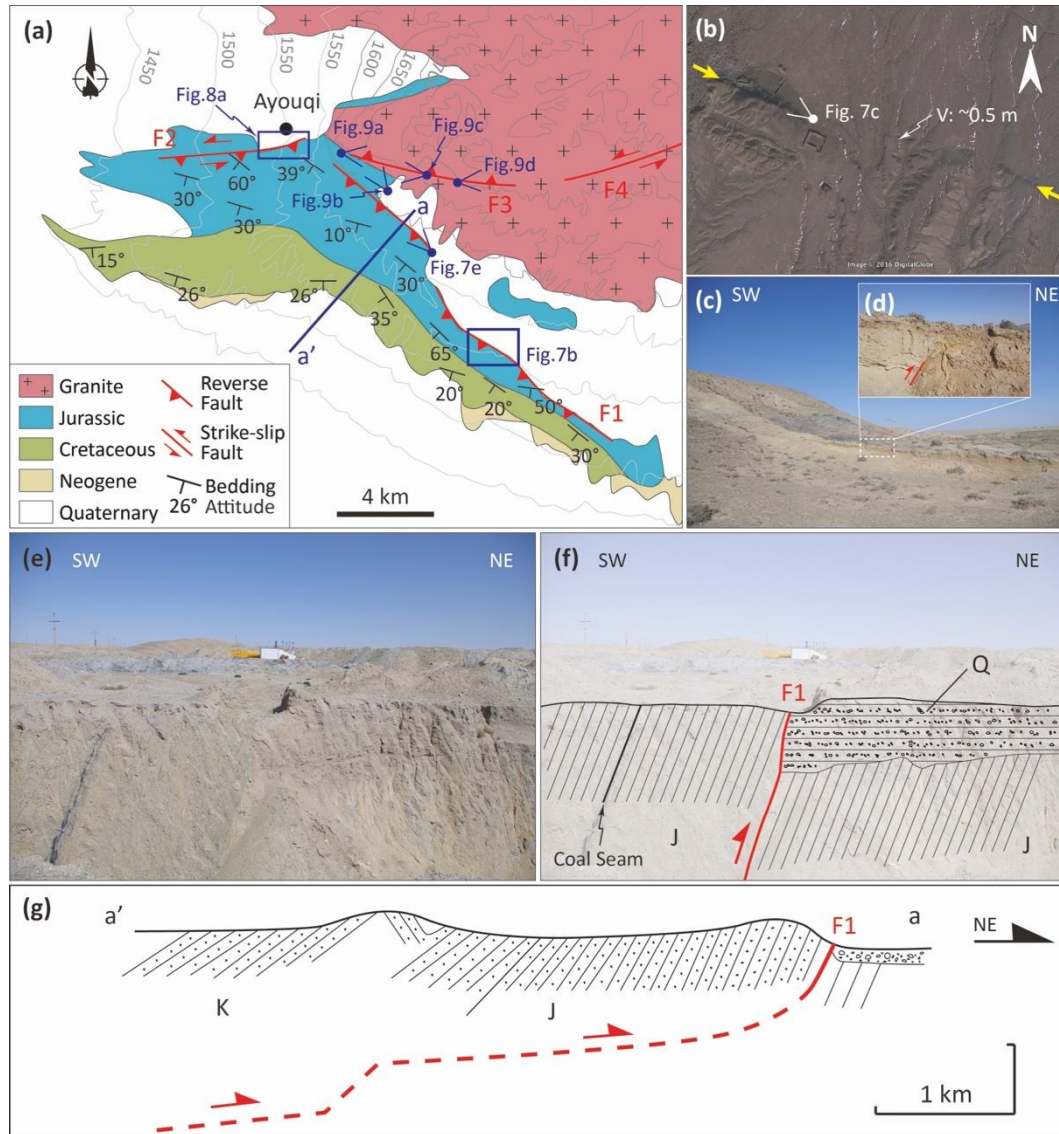


Fig. 7. (a) Geological map near Ayouqi county, showing exposed units and locations of the faults. Map compiled from GBGMR (1989). Location is shown in Fig. 6; (b) Google Earth imagery shows fault scarps on the alluvial-fan surface. Yellow arrows indicate the locations of fault scarp. See location in Fig. 7a; (c) Photograph showing fault scarp and a trench exposure. See location in Fig. 7b; (e) and (f) Fault exposure indicating that the Jurassic sandstone thrusts over the Quaternary conglomerate. See location in Fig. 7a; (g) An inferred geological transect. Transect location is shown in Fig. 7a.

Figure 8

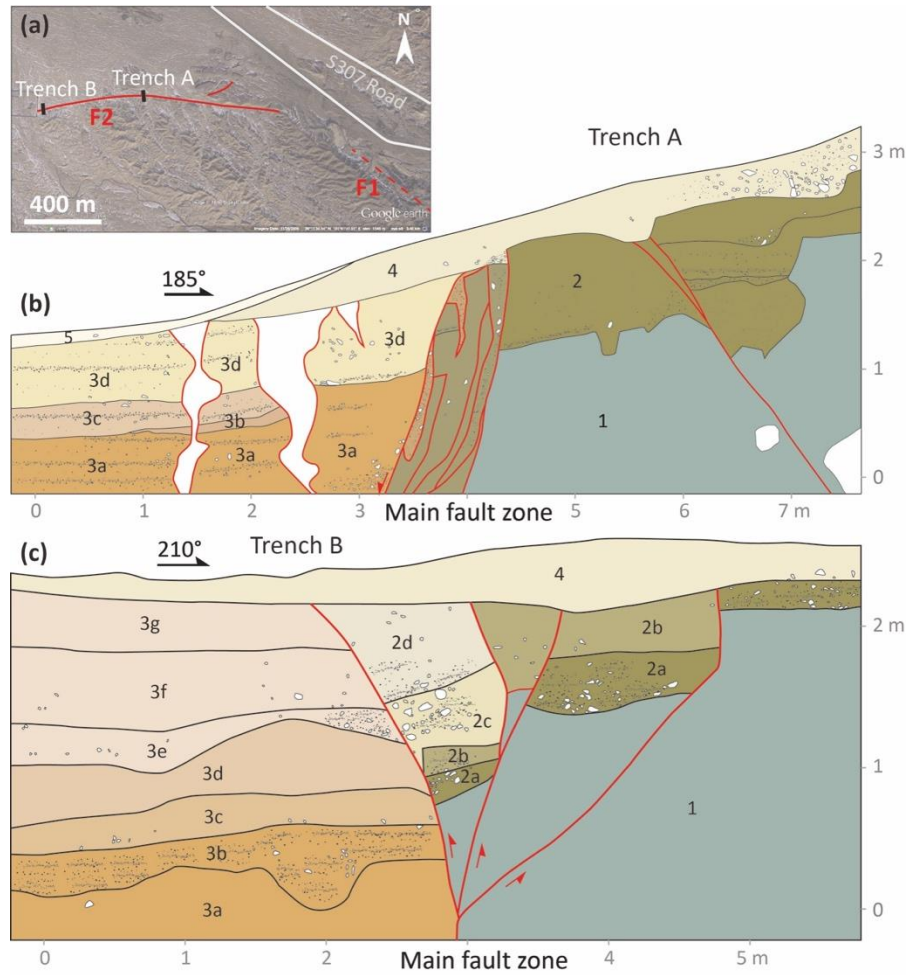


Fig. 8. (a) Google Earth imagery showing the fault F2 and locations of two trenches, Trench A and Trench B. See location in Fig. 7a; (b) and (c) are the sketches of the east walls of Trench A and Trench B, respectively. Unit label numbers correspond to discussion in text.

Figure 9

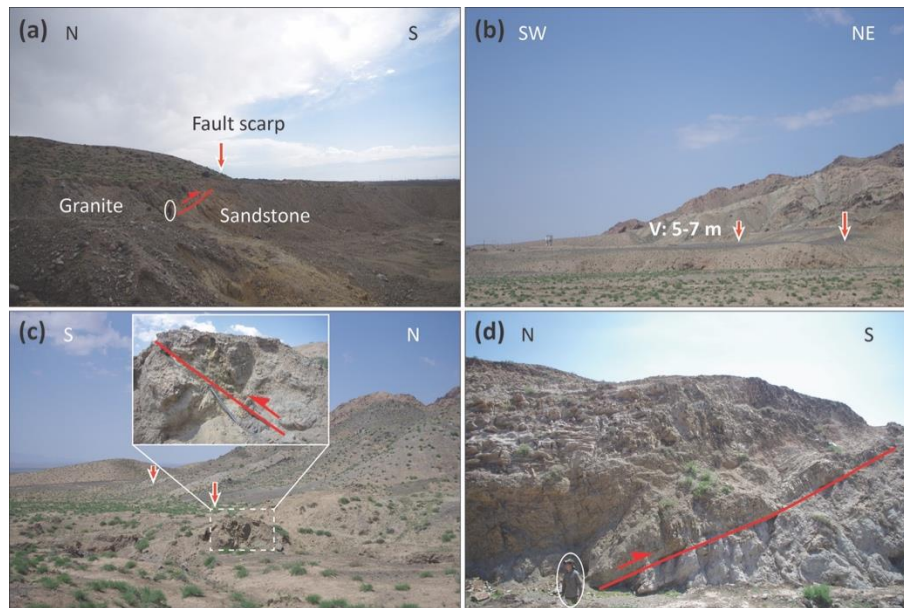


Fig. 9. Photographs of fault scarps and exposures along the fault F3. Perspectives of photos is annotated in Fig. 7a.

Figure 10

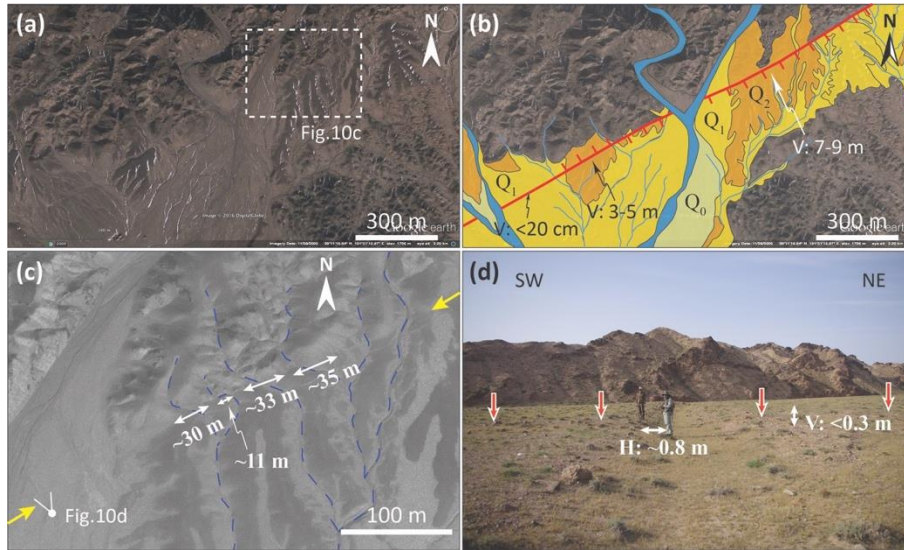


Fig. 10. (a) Google Earth imagery and (b) interpretive map of the western segment of the fault F4. See location in Fig. 6. Red lines show the locations of fault scarps and ticks indicate dips of fault scarps. Q_0 is active floodplain; (c) WorldView satellite imagery showing several gullies are offset in sinistral sense of motion. Yellow arrows indicate the location of fault scarp. See location in Fig. 10a; (d) Photograph showing a tiny stream was offset by ~ 0.8 m laterally and the vertical displacement on alluvial surface is < 0.3 m. See location in Fig. 10c.

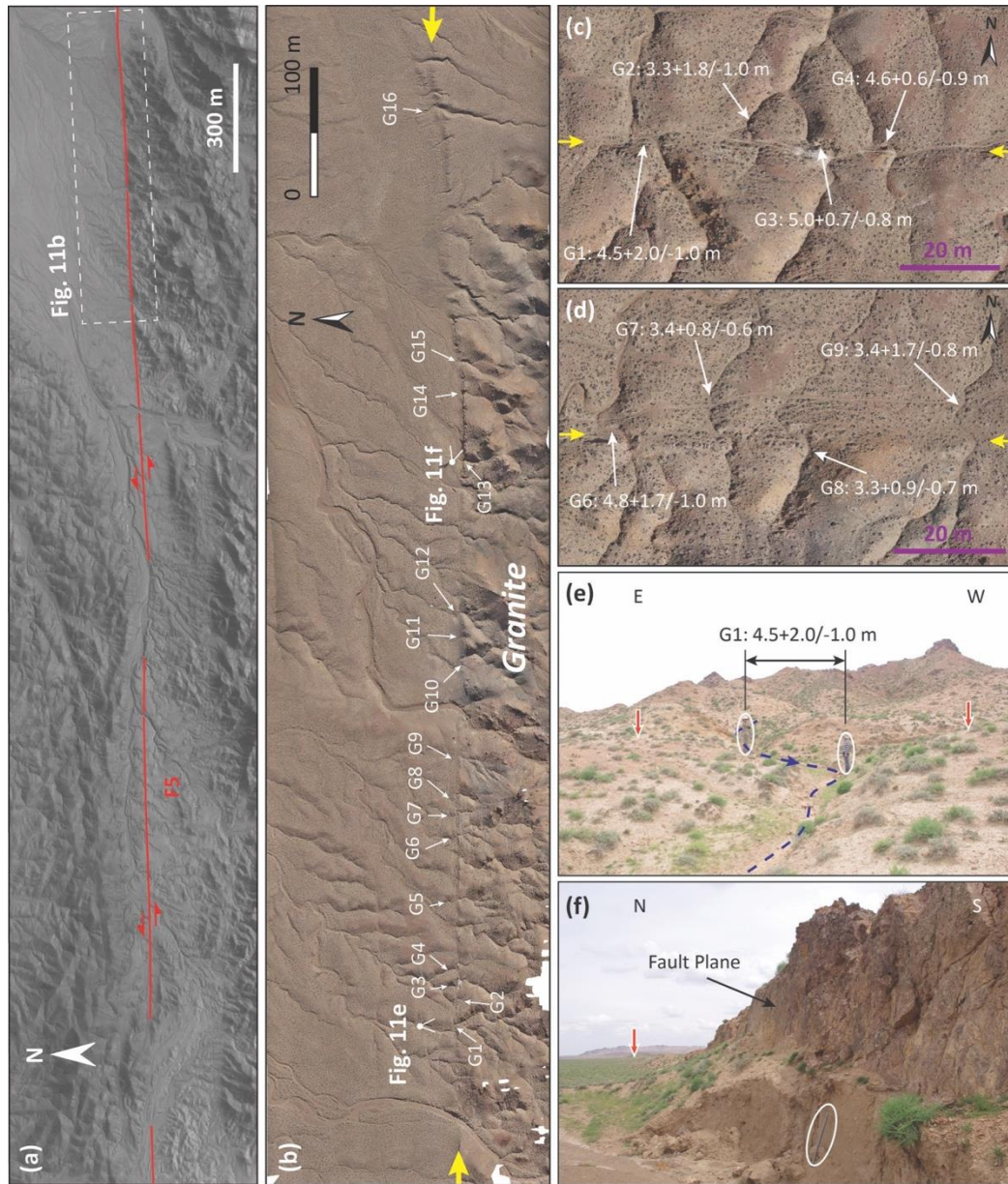
Figure 11

Fig. 11. (a) Pleiades satellite imagery suggests that the fault F5 expressed as a straight line, cutting alluvium with nearly no vertical displacement. Location is shown in Fig. 6; (b) Orthoimage shows 16 gullies are consistently offset in sinistral sense of motion in less than 1 km. Yellow arrows indicate location of fault scarp. See location in Fig. 11a; (c) and (d) Orthoimages show several gullies are offset by ~3-5 m; (e) Photograph showing the gully G1 was offset by ~4.5 m. Red arrows indicate the location of fault scarp; (f) Exposed fault plane with vertical dipping. Perspective of photo is annotated in Fig. 11b.

Figure 12

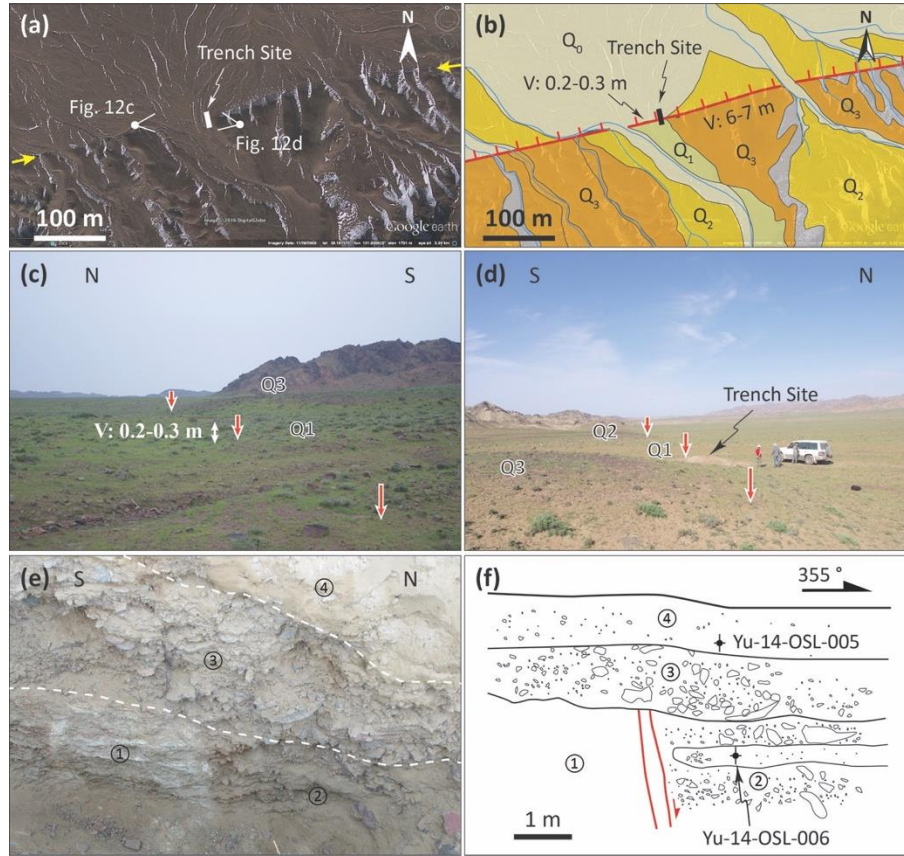


Fig. 12. (a) Google Earth imagery and (b) interpretive map in the western segment of the fault F5. Location is shown in Fig. 6; (c) and (d) Photographs showing displaced alluvial fans and the youngest fault scarp on the alluvial fan Q_1 . Perspectives of photos is annotated in Fig. 12a; (e) and (f) A trench exposure excavated across the fault scarp on Q_1 , Showing normal faulting. Trench location is shown in Fig. 12a, b.

Figure 13

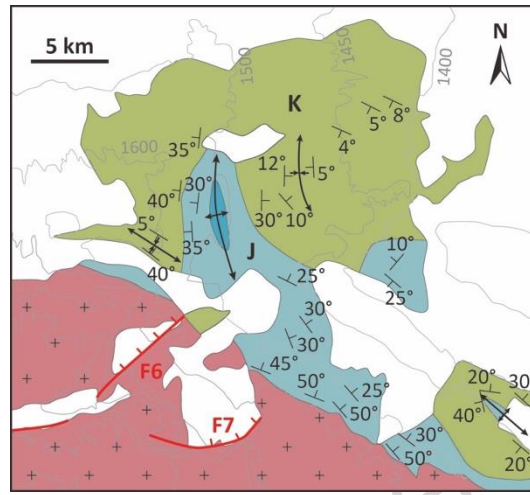


Fig. 13. Geological map at the eastern end of the Ayoubi fault zone. Red lines showing the locations of fault scarps and ticks indicate dips of fault scarps. See location in Fig. 6.

Figure 14

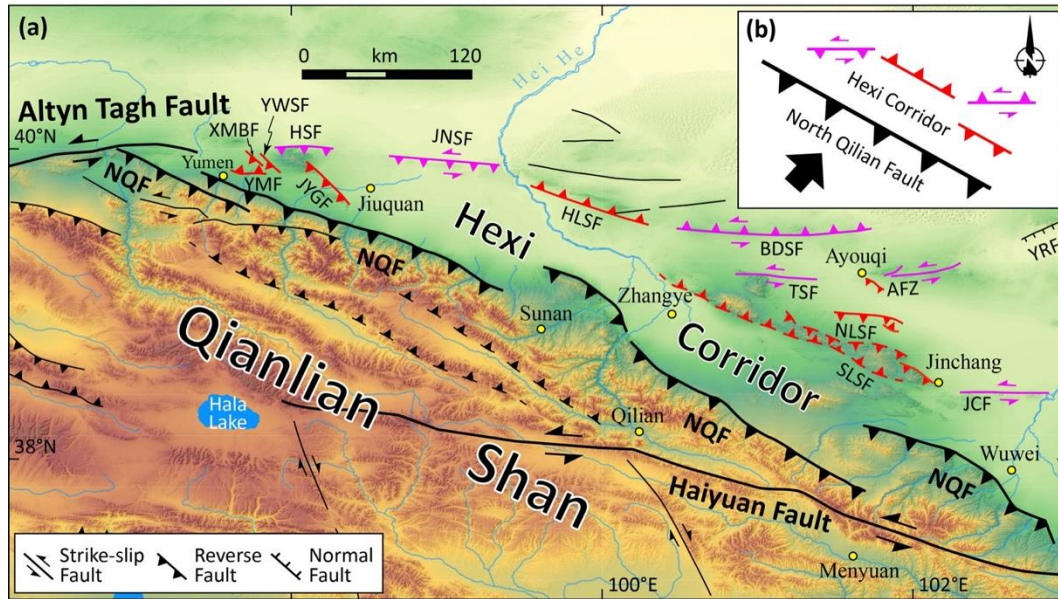


Fig. 14. (a) Tectonic map showing major and minor active faults in northern Tibet and the Hexi Corridor. Faults trending NW or NWW are shown in red, and faults with E-W trend are in purple; (b) Simplified geological deformation model in the Hexi Corridor. Abbreviations are as follows. NQF-North Qilian fault; YMF-Yumen fault; XMBF-Xinminbu fault; YWSF-Yinwa Shan fault; HSF- Hei Shan fault; JYGF-Jiayuguan fault; JNSF-Jinta Nan Shan fault; HLSF-Heli Shan fault; BDSF-Beida Shan fault; TSF-Taohuala Shan fault; AFZ-Ayouqi fault zone; NLSF-North Longshou Shan fault; SLSF-South Longshou Shan fault; JCF-Jinchang fault; YRF-Yabrai Range-front fault.

Table 1 Exposure ages of Alluvial-fan surfaces at the Taohuala Shan fault

Sample ID	Lab. ID	Lat (°E)	Lon. (°N)	El. (m)	Production rate (atoms/g/yr)	Pure quartz (%)	Spike (ml)	$^{10}\text{Be}/^9\text{Be}$	Uncertainty $^{10}\text{Be}/^9\text{Be}$ (%)	Age (ka)	Uncertainty (ka)
Yu-14-	XA-	39.	101.	16	14.65	30.354	0.314	2.97E-	0.97	137	12.0
Yu-14-	XA-	39.	101.	16	14.40	30.117	0.314	1.42E-	1.70	67.	5.9
Yu-14-	XA-	39.	101.	16	14.38	26.408	0.318	1.08E-	1.18	57.	4.9
Yu-14-	XA-	39.	101.	16	14.35	25.673	0.318	1.09E-	1.17	59.	5.1
Yu-14-	XA-	39.	101.	16	14.33	25.176	0.318	5.29E-	2.89	29.	2.7

Note: 1. Samples were processed and tested in Xi'an Accelerator Mass Spectrometry Center (XAAMS); 2. Production rates are from Lal (1991)/Stone (2000); 3. A density of 2.65 g cm⁻³ and a thickness of 2 cm were used for all surface pebble samples; 4. $^{10}\text{Be}/^9\text{Be}$ measured against standards derived from NIST SRM 4325, with an assigned ratio of 2.68E-11.

Table 2 Dating results from optically stimulated luminescence samples

Sample ID	Depth (m)	U (ppm)	Th (ppm)	K (%)	Water content (%)	Dose rate (Gy/ka)	Equivalent dose (Gy)	Age (ka)
Yu-15-OSL-001	0.95	1.80	6.94	2.19	5 ± 3	3.30 ± 0.11	91.99 ± 1.85	27.90 ± 1.09
Yu-15-OSL-005	0.50	2.32	9.68	1.89	5 ± 3	3.98 ± 0.14	16.15 ± 0.98	4.06 ± 0.29
Yu-15-OSL-006	2.40	2.10	8.65	1.80	5 ± 3	3.05 ± 0.09	33.70 ± 1.23	11.05 ± 0.52

Note: The content of U, Th, and K₂O measured by inductively coupled plasma-atomic emission spectroscopy (ICP-AES) at the University of London. OSL samples measured by the State Key Laboratory of Loess and Quaternary Geology, Institute of Earth Environment, Chinese Academy of Sciences.

Highlights:

1. The Taohuala Shan-Ayouqi fault zone is characterized by left-lateral strike slip with a reverse component;
2. The most recent earthquake in the Ayouqi fault zone occurred between ca. 11.05 ± 0.52 ka and ca. 4.06 ± 0.29 ka;
3. Left-lateral strike-slip faults in the Hexi Corridor are associated with the northeastward extrusion of north Tibet and do not link with the Altyn Tagh fault.